EUROPEAN ORGANIZATION FOR NUCLEAR RESEARCH

CERN-EP/82-37
31 March 1982

CALORIMETRY IN HIGH-ENERGY PHYSICS

C.W. Fabjan
CERN, Geneva, Switzerland

T. Ludlam
Brookhaven National Laboratory, Upton, NY, USA

Submitted to
Annual Review of Nuclear and Particle Science

CONTENTS

1. INTRODUCTION

The detection of particles is the experimental tool of high-energy physics research, and the evolution of the field has been closely coupled to the development of improved methods for detecting and measuring an ever-widening spectrum of particle properties.

Much of our present knowledge about the physics of elementary particles has been the result of a continuing refinement of techniques for measuring the trajectories of individual charged particles — from the early hodoscopes, cloud chambers, and emulsion stacks, to today's extraordinarily precise bubble and streamer chambers and sophisticated magnetic spectrometers, equipped with multiwire proportional or drift chambers (Charpak et al 1978, Fabjan & Fischer 1980).

In this article we examine an intrinsically different class of detector which has come to the fore over the past decade and promises to greatly influence the scope of future experiments — total absorption detectors, or calorimeters.

Conceptually, a calorimeter is a block of matter, which intercepts the primary particle and is of sufficient thickness to cause it to interact and deposit all its energy inside the detector volume in a subsequent cascade or "shower" of increasingly lower energy particles. Eventually most of the incident energy is dissipated and appears in the form of heat. Some (usually a very small) fraction of the deposited energy goes into the production of a more practical signal (e.g. scintillation light, Čerenkov light, or ionization charge) which is proportional to the initial energy. In principle, the uncertainty in the energy measurement is governed by statistical fluctuations in the shower development, and the fractional resolution σ/E improves with increasing energy E as $1/\sqrt{E}$.

The first large-scale detectors were used in cosmic-ray studies (Murzin 1967). Interest in calorimeters grew in the late 1960's and early 1970's in view of the coming machines (CERN-ISR, Fermi National Accelerator Laboratory, CERN-SPS) with their greatly changed experimental environments, making, for example, magnetic momentum analysis in large solid-angle experiments increasingly difficult (Atač 1975).

This period corresponded also to the advent of intense, high-energy neutrino beams with the need for very massive detectors to study their interactions. Not surprisingly, this detector development was paralleled by the rapid growth of analogue-signal processing techniques: during the last decade the typical number of analogue-signal channels of nuclear spectroscopy quality has increased from about 10 to 10^4 in high-energy physics experiments!

At the outset it was noted that calorimetric detectors offer many other attractive capabilities, aside from the energy response, all of which have since been exploited in varying degrees:

- they are sensitive to neutral as well as charged particles;
- the size of the detector scales logarithmically with particle energy E, whereas for magnetic spectrometers the size scales with $\sqrt{p}$, for a given relative momentum resolution $\Delta p/p$;
- with segmented detectors, information on the shower development allows precise measurements of position and angle of the incident particle;
- the differences in response to electrons, muons, and hadrons can be exploited for particle identification;
- their fast time-response allows operation at high particle rates, and the patterns of energy deposition can be used for real-time event selection.

We are now entering an era in which high-energy colliding beam machines may reveal a "new" physics of super-massive particles (Ellis 1981) in extremely rare and complex events, and whose signatures include the production of very energetic leptons and the fragmentation of massive quarks. In these experiments the traditional momentum analysis of a few charged particles will be replaced by measurements of momentum and energy flow among multiple jets of particles. Calorimetric detectors are uniquely suited to such tasks, provided the intrinsic potential of these instruments as primary detectors can be fully realized.

In Section 2 we survey the calorimeter installations which have been introduced into a variety of high-energy physics experiments. We describe the physics requirements which lead to finely instrumented total absorption detectors for neutrino experiments and investigations of nucleon stability, followed by a summary of the uses of calorimeters for the detection of multiparticle final states in experiments with hadron and electron beams.

In Section 3 we review the physics of the cascade development for electromagnetic and hadronic showers in dense materials, emphasizing the measurements and calculational techniques of properties which govern the performance of calorimeters. This is followed, in Section 4, by a discussion of the detector parameters which relate to the intrinsic performance and implementation for specific experimental applications: the resolving power for energy; position and angle measurements; timing properties; the capability for particle identification; and factors such as calibration and monitoring of large detector systems. In Section 5 we examine the methods of readout employed for calorimetric measurements.

Finally, we summarize the state of the art, point to specific trends of development, and assess the potential of the calorimetric methods for future physics programs.

We have aimed at presenting a broad view of the role of calorimeters in high-energy physics and have preferred to illustrate our important points with representative examples. This review is therefore not rigorously complete, and it is suggested that recent excellent discussions be consulted (Iwata 1979, Albrow 1981, Amaldi 1981, Astbury 1981, Gordon et al 1981).

2. CALORIMETER SYSTEMS FOR PHYSICS APPLICATIONS

2.1 Neutrino Physics and Nucleon Stability

Detectors for these studies share a number of common features: the event rate is low and proportional to the total instrumented mass; the physics requires a fine-grained readout system, which permits detailed three-dimensional pattern reconstruction. Bubble chambers have therefore been used extensively but lack sensitivity owing to their limited mass. The present generation of neutrino detectors makes extensive use of wire-chamber techniques to approach the intrinsic spatial and angular resolution of calorimeters. New "visual" electronic techniques are being developed for proton decay experiments, for which the most massive detectors with the highest density of signal channels are required.

2.1.1 NEUTRINO DETECTORS The size of these detectors is governed by the cross-section for neutrino interactions, $\sim 10^{10}$ times smaller than hadronic cross-sections. Even with intense neutrino beams, the detector must have a very large mass (typically many hundreds of tons), and its volume must be uniformly sensitive to the signature that an interaction has occurred and to the characteristics of the reaction products. These requirements explain the modular construction typical of modern electronic neutrino detectors, of which two examples are shown in Figure 1. Each calorimeter module consists of several planes of dense absorber interleaved with planes of detectors to record the pattern of charged particles emerging from the absorber layers. The detector planes are subdivided into a sufficiently fine-grained array of independent readout cells to allow adequate pattern recognition. The general form of the interaction is $\nu_{(\mu,e)}$ + nucleon = $\ell_{(\mu,e)}$ + X, where ℓ is a charged lepton (charged-current interaction) or a neutrino (neutral-current interaction), and X represents the system of recoiling hadrons projected forward into a collimated jet by relativistic kinematics. In the simplest instance the signature for a neutrino interaction is the sudden appearance of a large amount of energy in a few layers, deep in the detector. If the scattered lepton is a muon, it leaves in each detector layer the characteristic signal of a single minimum-ionizing particle. In some detectors the absorber layers are magnetized iron, which makes possible a determination of the muon momentum from the curvature of its trajectory. (For an example, see Figure 22.) For the detailed study of neutral-current interactions a very fine-grained subdivision of the calorimeter system is required for measuring the energy and direction of the hadronic system X and for reconstructing the "missing" momentum of the final-state neutrino.

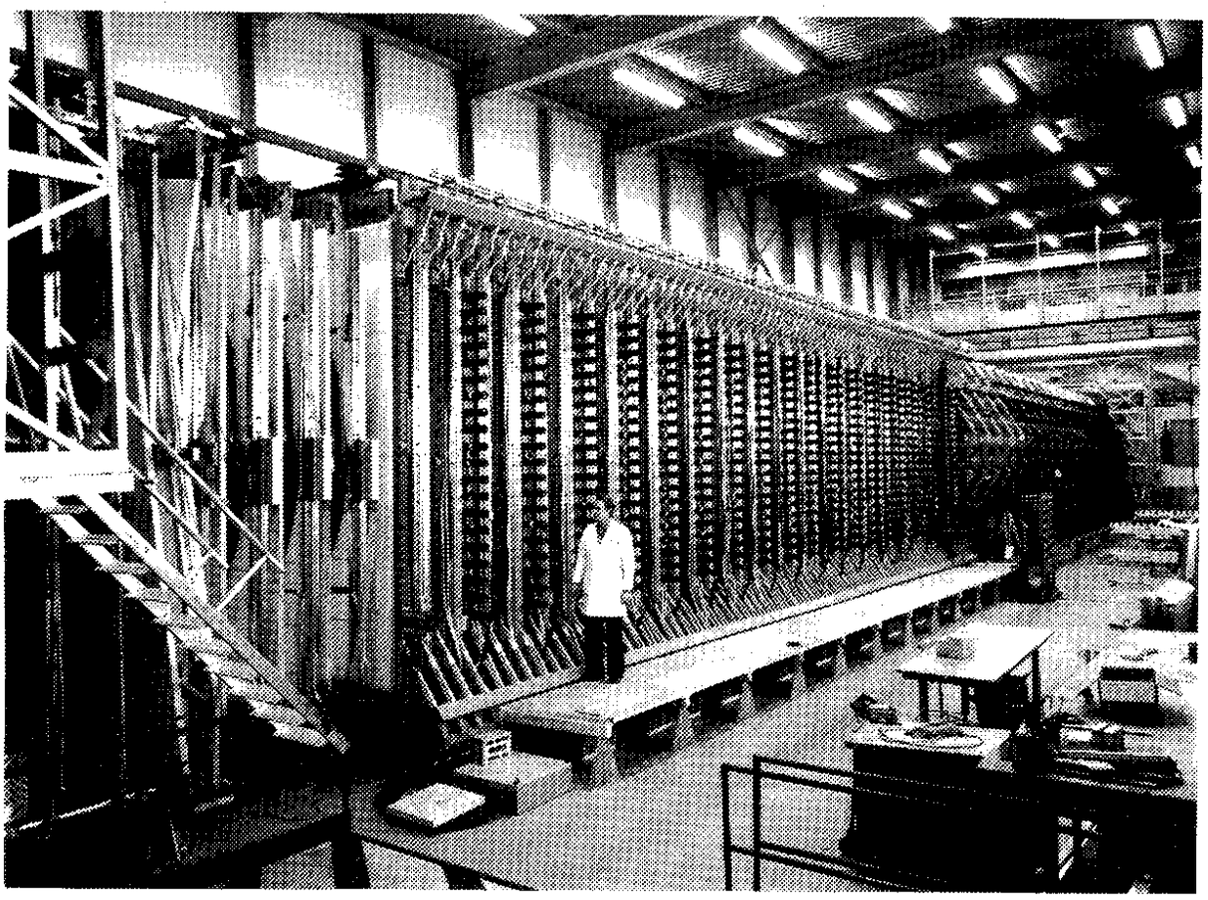

Figure 1 The two counter neutrino facilities at CERN. The ν beam enters first the CDHS experiment (in the background) and subsequently the apparatus of the CHARM Collaboration. Both experiments are based on very massive, highly modular scintillation calorimeters, and measure particle position with wire-chamber techniques (Photo CERN).

Clearly the scope and sensitivity of neutrino experiments would be much improved if even the most massive detectors could resolve final-state particles with the reliability and precision typical of a bubble chamber. With this goal in mind, some schemes are currently being investigated which use drift chamber methods with large volumes of compressed gas, providing a visual quality characteristic of homogeneously sensitive detectors. In one case (Vishnevskii et al 1979) a cylindrical detector 3.5 m in diameter and 35 m long is envisioned, containing about 100 tons of argon gas at 150 atm pressure, with ionization electrons collected on planes of anode wires. The idea has also been advanced (Bouclier et al 1980) of using compressed mixtures of more common gases (air or freon) or room-temperature liquid hydrocarbons (private communication, Willis 1980), and detecting the ions which migrate away from charged particle tracks (positive ions and/or negative ions produced by electron attachment). Many technical problems need further study before these ideas can be realized in practical detectors.

Closely connected with neutrino physics is a class of investigations referred to as "beam dump" experiments. Here, intense beams of protons are directed at an inert, massive absorber (the beam dump), capable of fully containing the hadronic reaction products. A detector downstream from this absorber is used to compare the fluxes of emerging muons and neutrinos with that of the incident hadrons. The observed leptons are presumed to be products of the weak decay of particles produced by the interacting protons. The results can be corrected for the lepton flux due to pions and kaons, which decay before interacting in the absorber. An excess of leptons is observed, which gives evidence for additional families of particles with much shorter lifetimes. Such experiments gave an early indication of the hadronic production of charmed particles (Dydak 1980, Derrick 1981).

2.1.2 NUCLEON STABILITY The possibility of nucleon decay has been studied experimentally for several decades. Recently, these efforts have received a strong impetus from "grand unified theories" of weak, electromagnetic, and strong interactions which provide definite predictions of the nucleon lifetime (Georgi et al 1974, Pati & Salam 1974, Ellis 1981). Present estimates place the proton lifetime around $\tau_p \simeq 10^{31\pm2}$ y, about three orders of magnitude above the current experimental limit of $\tau_p \simeq 10^{28}$ y (Krishnaswamy et al 1981) and barely within reach of present experimental finesse. To achieve a limit of about 10^{32} y, approximately 1000 tons, containing 10^{33} nucleons, have to be instrumented to search sensitively for some of the expected decay modes such as: $p \rightarrow e^+ + h^0$, where h^0 is a neutral meson ($\pi^0, \eta, \rho^0, \omega^0$, etc.). The signature of such a decay is rather striking but requires a detector with sufficient subdivision to recognize the back-to-back decay into a lepton and a hadron with the relatively low energy deposit of about 1 GeV. The sensitivity is limited by the flux of muons and neutrinos originating from atmospheric showers. Only μ's can be shielded by placing the experiments deep underground in mine shafts or in road tunnels beneath Alpine mountains. The ν-induced rate simulating nucleon decay is estimated at $\sim 10^{-2}$ events per ton per year if energy deposition alone is measured. If complete event reconstruction is possible, a further suppression of about 100 may be achieved and one may reach an experimental limit of $\tau \gtrsim 10^{33}$ y (Goldhaber & Sulak 1981, Treille 1981). Section 2.3 gives further information.

2.2 Storage Ring Experiments

The apparent lack of driving physics motivations paired with major technical difficulties was not propitious for a vigorous development of calorimeters at storage rings: such detectors are large, complex, and costly, because most of the solid angle has to be covered in a complicated (approximately spherical) geometry and adequately instrumented (Figures 2 and 3). Only now have electromagnetic calorimeters become relatively "standard" detectors, whereas hadronic calorimeter facilities are still quite rare. Beautiful Gedanken experiments have therefore preceded reality by more than a decade (Willis 1972).

Most of our comments, which we illustrate with storage ring applications, apply also to the use of calorimeters for fixed-target experiments. Several pioneering studies at FNAL (Bromberg 1979, Dris et al 1979) and at the CERN-SPS (Pretzl 1981) have contributed to improving the understanding of calorimetry in hadronic physics and have found unexpected and striking results on the production cross-section and topology of events with a large transverse energy.

2.2.1 PHYSICS APPLICATIONS At *hadron machines* the studies focus on reactions that are characterized by a large transverse energy flow, as a signal for a highly inelastic interaction between the nucleon constituents. The signature appears in many different characteristic event structures and may therefore be efficiently selected with hadron calorimeters: examples are single high-$p_T$particles, "jets" of particles, or events exhibiting large transverse energy E_T irrespective of its detailed structure. Topical applications include invariant mass studies of multijet systems. This is considered as a possible strategy that could be used to search for a $t\bar{t}$ signal, because two- or three-jet decays may dominate over the $\mu^+\mu^-$ channel by a factor $\gtrsim 100$. Further motivation for this "jet spectroscopy" is provided by the gauge theories of elementary particles (Bég 1981), stipulating new particles in the 10–100 GeV mass range, which are expected to decay with a characteristic pattern of several jets. Apart from these studies which are being pursued with present detectors at the CERN ISR and the $p\bar{p}$ collider, and which influence the design of future detectors for ISABELLE and the $p\bar{p}$ collider at FNAL, hadron calorimeters are considered to be most essential in studies of ultrarelativistic heavy-ion collisions (Willis 1981). As an example, in collisions between nuclei with $A \gtrsim 100$ and ~ 20 GeV per nucleon, several thousands of particles may be produced, carrying a total of several thousand GeV. Except for small-solid-angle, special-purpose detectors, probably only calorimeters will provide meaningful measures of such events, which are too complicated at the individual-particle level although suitable averages may reveal striking signatures.

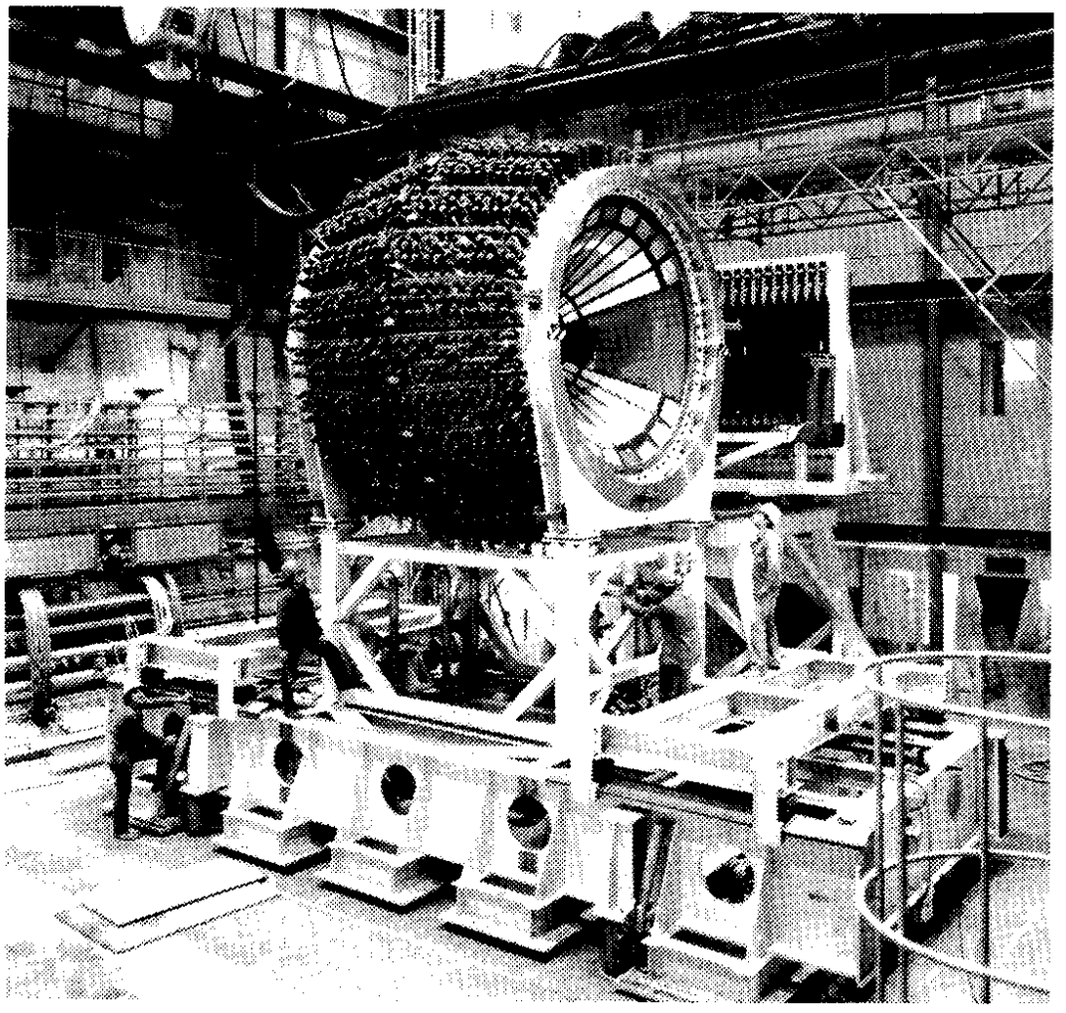

Figure 2 View of the hadron calorimeter of the UA2 Collaboration at the CERN $p\bar{p}$ collider. This spherical detector is made from 24 "orange"-like segments, containing 10 cells with threefold longitudinal subdivision (Photo CERN).

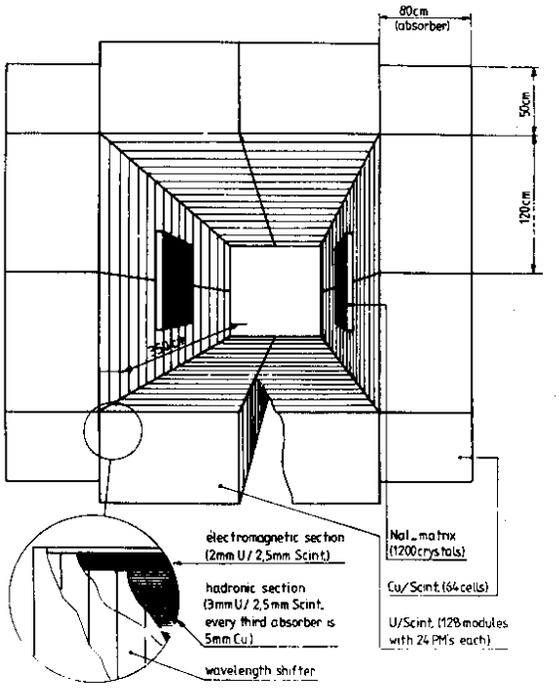

Figure 3 Isometric view of the AFS uranium calorimeter at the CERN ISR. The 8 sr detector is subdivided into 800 cells with four readout channels each. Also shown are two high-granularity NaI "crystal walls", with a total of 1200 readout channels.

At *electron-positron colliders*, electromagnetic detectors are frequently used to measure the dominant fraction of neutral particles, π^0's. They are also the ideal tool for detecting electrons, which may signal decays of particles with one or more "heavy" (c,b,...) quarks. Unique investigations of $c\bar{c}$ and $b\bar{b}$ quark spectroscopy were accomplished with very high resolution NaI-type shower detectors (Scharre 1981, Schamberger 1981).

Many features of the physics program at the next generation of e^+e^- colliders [LEP (Picasso 1981), SLAC Linear Collider (Panofsky 1981), CESR II (McDaniel 1981)] will require the extensive use of hadronic calorimeters (Cundy et al 1976, Willis & Winter 1976, Fabjan 1980).

In particular, the characteristic feature of $e^+ e^-$ annihilation — production of particles at relatively large angles with a total energy equal to the centre-of-mass collision energy — makes the experimental technique of Total Energy Measurement particularly appropriate. For future e^+e^- physics this method will be important because

a) the level of neutron and K_L^0 production, measurable only with hadronic calorimeters, is expected to increase with energy;

b) a large and most interesting fraction of events will contain neutrinos in the final state; missing energy and momentum analysis provides the sole handle on such reactions;

c) a considerable fraction of events will show good momentum balance but large missing energy; these may be two-photon events or, above the Z^0 pole, events on the radiative tail. Total energy will provide the cleanest signature.

d) $e^+e^- \rightarrow W^+W^-$: hadronic calorimeters will be the most powerful tool for measuring this reaction, either in channels where each W decays hadronically (total of four jets) or through the rarer leptonic decay channels.

2.2.2 CONSEQUENCES OF DETECTOR LIMITATIONS Energy and space resolution are the principal calorimeter properties which affect the physics studies. Consider as an example a typical multijet event of 200 GeV which can be measured with an accuracy of $\sigma \approx 6$–8 GeV. Likewise, the total momentum balance can be checked at a level of $\sigma \approx 4$ GeV/c (Cundy et al 1976). These are intrinsic performance figures, disregarding possible instrumental effects (see Section 5) and are well matched to the next generation of e^+e^- programs. While such a performance is also adequate for work at hadronic machines, a further serious difficulty arises from the convolution of the *energy response function* with the steeply falling p_T distribution of hadronically produced secondaries (Selove 1972, Almehed et al 1977, Block 1977, Dris 1979). As a consequence (see Figure 4), the measured energy deposit E_m in the detector will originate predominantly from incident particles with energy $E < E_m$; therefore count rates and trigger rates are higher than the true physics rates. The result can be devastating for detectors with poor energy resolution or a non-Gaussian response function ("tails" in energy resolution), making the deconvolution almost impossible. The problem is compounded by the tendency to respond to π^0's with a signal larger than that from charged pions (see Sections 3 and 4). Without adequate precautions, these detectors would preferentially select π^0's, rendering them useless for general trigger applications.

The *granularity* of the detector characterizes the spatial separation between two particles in an event. The required degree depends on the minimum angle θ to be detected between particles and is therefore imposed by the physics. An example is the individual detection of some or most of the particles inside a jet, e.g. the detection of an electron inside such an event. Showers have to be separated by approximately one shower diameter d to be recognized individually, which therefore defines the minimum distance D of the detector from the interaction point as $D \gtrsim d/\theta$. As the total instrumented volume of the calorimeter scales approximately with $\sim D^3 \sim d^3$, one might pay a premium for a high-density detector and still achieve the over-all most economical design, provided the distance scaling is correctly implemented.

The granularity requirement dominates the *size* consideration for calorimeters. In contrast, the c.m. energy of the collider imposes a weaker scaling of the size: for full shower containment the thickness of the detector scales logarithmically with energy and increases by a factor of 2 from E = 10 GeV to 100 GeV.

The *trigger capability* is a unique, and perhaps the most important, requirement of hadron calorimeters employed at hadron machines. For satisfactory operation, one needs: uniform response irrespective of event topology and particle composition; good energy resolution at the trigger level to minimize effects of the response function; adequate granularity at the trigger level for selection of specific event topologies. For high selectivity, rather complex analogue computations are required, as may be gleaned from the examples in Table 1 (Rosselet 1981).

2.3 Calorimeter Systems

In Table 2 we have summarized information on some calorimeter facilities. This incomplete selection emphasizes the great variety of applications, techniques, and performances. (CDHS: Abramowicz et al 1981; CHARM: Diddens et al 1980; FNAL Exp 594: Bogert et al 1981; BNL Exp. 734: Amako 1981; Fréjus: Barloutaud 1981; IMB: Van der Velde 1981; NA5: Eckardt et al 1978; Mark J: Davies-White et al 1979; CELLO: Behrend et al 1981; AFS: Botner et al 1981a; UA1: Corden et al 1982; UA2: Clark et al 1982; MAC: Anderson et al 1978).

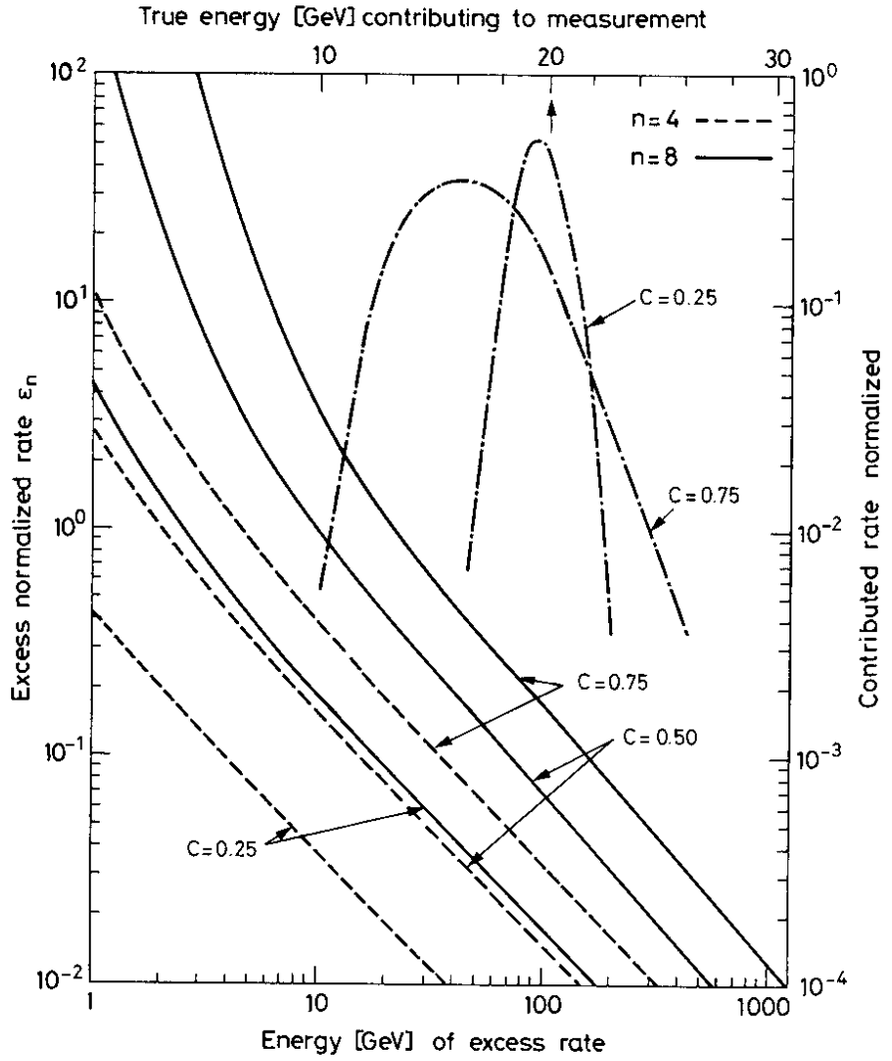

Figure 4 The results (left ordinate versus bottom abscissa) of the convolution $\tilde{S}(E_0) = \int_{E_1}^{\infty} S(E) \cdot R(E,E_0)\, dE$ of a *Gaussian* energy response function $R(E,E_0) = [1/\sqrt{2\pi}\,\sigma(E)] \exp - (E - E_0)^2/2\sigma^2(E)$, $\sigma(E) = c\sqrt{E}$, with a spectrum $S(E) = A/E^n$. The excess normalized rate is given by $\varepsilon_n = [\tilde{S}_n(E_0) - S_n(E_0)]/S_n(E_0)$. Also shown (dashed-dotted curve corresponding to right ordinate versus top abscissa for $n = 8$) is an example of the corresponding energy distribution, which contributes to an energy measurement of $E_0 = 20$ GeV. Due to the steep fall $\sim E^{-n}$, the most probable energy E contributing may be substantially lower than E_0 (adapted from Block 1977).

Table 1 Triggering with hadron calorimeters

Experiment	Trigger
Single-particle inclusive distr., correlations	Localized energy deposit in spatial coincidence with matching track; several thresholds used concurrently.
Jet studies	Extended ($\sim$ 1 sr) energy deposit; several thresholds and multiplicities.
Inclusive leptons, multileptons	Electromagnetic deposit in spatial coincidence with matching track; several thresholds and multiplicities.
Flavor jets	Jet trigger with additional lepton required.
Correlations	Various combinations of above triggers.

Table 2 Examples of calorimeter facilities

Logo	Major physics goals	Size (t) (approx.)	Technique	No. of read-out channels	σ_E (for 1 GeV) Hadrons	Photons	Comment
CDHS	ν physics; emphasis on structure functions	1400	2.5 cm or 5 cm Fe plates sampled with scintillators and drift chambers	3600 PMs 4000 drift wires	58(70)% 2.5(5)cm	23%	
CHARM	ν physics; emphasis on neutral-current events	150	8 cm marble plates sampled with scintillator and proportional tubes	$\sim$ 1600 scintillators $\sim 10^4$ prop. tubes	53%	20%	Optimized for angular resolution for missing momentum determination.
FNAL Exp. 594	ν physics	340	Flash tubes between layers of sand and steel pellets	$\sim 4 \times 10^5$ flash tubes	80%	10%	Very fine-grained readout for optimum pattern recognition.
BNL Exp. 734	ν physics	120	Homogeneous liquid scintillator, proport. tubes	3800 PMs 13,000 prop. tubes	Not available		Active absorber for optimum sensitivity to elastic scattering events.
Fréjus	Nucleon stability	1500	Iron, flash tubes	$\sim 10^6$	$\sigma \approx 15\%$ expected for $p \rightarrow e^+\pi^0$		
IMB	Nucleon stability	7000	Homogeneous water Čerenkov detector	1350 8 in. dia. PMs	$\sigma \approx 20\%$ expected for $p \rightarrow e^+\pi^0$		Patterns of Č light give adequate spatial and energy resolution with largest feasible detector mass.
NA5	Hadronic high-p_T particle production	70	0.55 cm Pb/scintillator for e.m. part 5 cm Fe/scintillator for H part	500 PMs on wavelength shifters	86%	16%	Complete azimuthal coverage for bias-free triggering.
MARK J	Study of e^+e^- annihilation	180	0.5 cm Pb/scintillator for e.m. part Iron/scintillator for H part	Coarse readout with PMs Drift chamber	20% for 30 GeV events	10%	Coarse sampling, but almost complete 4π coverage.
CELLO	Study of e^+e^- annihilation	50	0.12 cm Pb/0.36 cm liquid argon	8000 charge amplifiers	–	9%	4π coverage with high-performance e.m. calorimeter.
AFS	Hadronic production of very high E_T states	300	0.2 cm U/0.25 cm scint. for e.m. part 0.3 cm U/0.25 cm scint. for H part	3200 PMs on wavelength shifters	35%	15%	Complete azimuthal coverage for bias-free triggering.
UA1	Hadronic production at $\sqrt{s} = 540$ GeV	1000	0.2–0.4 cm Pb/scint. for e.m. part 5 cm Fe/scintillator for H part	2200 PMs	75%	15%	4π coverage. Hadron calorimeter integrated with spectrometer magnet.
UA2	Hadronic production at $\sqrt{s} = 540$ GeV	100	3.5 mm Pb/scintillator for e.m. part 1.5 cm Fe/scintillator for H part	1700 PMs on wavelength shifters	60%	15%	Spherical geometry!
MAC	Study of e^+e^- annihilation	400	0.28 cm Pb/proportional tubes for e.m. part 2.7 cm Fe/proportional tubes for H part	10^5 wires grouped in 6000 signal channels	75%	17%	Calorimeter iron is magnetized for μ spectroscopy; nearly spherical geometry.

3. ENERGY LOSS IN DENSE ABSORBERS

3.1 Electromagnetic and hadronic showers

In this section we describe the properties of electromagnetic and hadronic showers. We emphasize the mechanisms contributing to fluctuations in the cascading process, which impose the fundamental limitations on calorimetric determination of the energy, position, and direction of particles. Characteristic properties describing the average behaviour of electromagnetic and hadronic showers are summarized in Table 3. One notes the remarkably different dependence on the absorber material, which reflects the very different nature of the two cascading processes.

Table 3 Average properties of electromagnetic and hadronic showers

Quantity	Electromagnetic showers	Hadronic showers
Mean free path	$9X_0/7$ for γ's $X_0 \simeq 180\ A/Z^2$ [g cm^{-2}]	$\lambda = A/(N_{Avogadro} \cdot \sigma_{Abs})$ $\propto A^{1/3}$
Secondary particles	e^+, e^-, γ; below critical energy $\varepsilon \simeq 550$ MeV/Z ionization loss only. Inelasticity $\kappa = 1$ (all energy given to particle production).	Fast nucleons, pions; medium-energy ($\sim$ 100 MeV) p's and n's; low-energy ($\sim$ 10 MeV) p, n, γ; nuclear fragments; inelasticity $\kappa \sim 0.5$.
Average shower dimensions		
Shower maximum*)	$t_{max}[X_0] \simeq \ln E\,[GeV]/\varepsilon\,[MeV] - \alpha$ ($\alpha \simeq 1$ for electr., $\simeq 0.5$ for γ's)	$t_{max}\,[\lambda] \simeq 0.6 \ln E - 0.2$
Depth for $\simeq$ 95% longitud. containment*)	$L_{0.95}[X_0] \simeq t_{max} + 0.08Z + 9.6$	$L_{0.95}[\lambda] \simeq t_{max} + 4E^{0.15}$ [GeV]
Radius for $\simeq$ 95% radial containment	$R \simeq 2\rho_M \simeq 14A/Z$ [g cm^{-2}]	$R \simeq \lambda$

*) Measured from face of calorimeter.

For electrons and photons the shower develops predominantly through bremsstrahlung and pair production. The scale for the longitudinal distribution is set by the "radiation length" (X_0) related to the mean path length of an electron in a material (A,Z). Through the multiplication process, the largest number of secondary particles is reached at a depth t_{max}, after which the number and energy of secondaries decrease with a characteristic attenuation length λ_{att}, which is determined by the mean free path of photons with energy corresponding to minimum absorption in the material (Figure 5). Eventually, the particles reach a "critical" energy, $\varepsilon \sim 550$ MeV/Z, below which no further multiplication

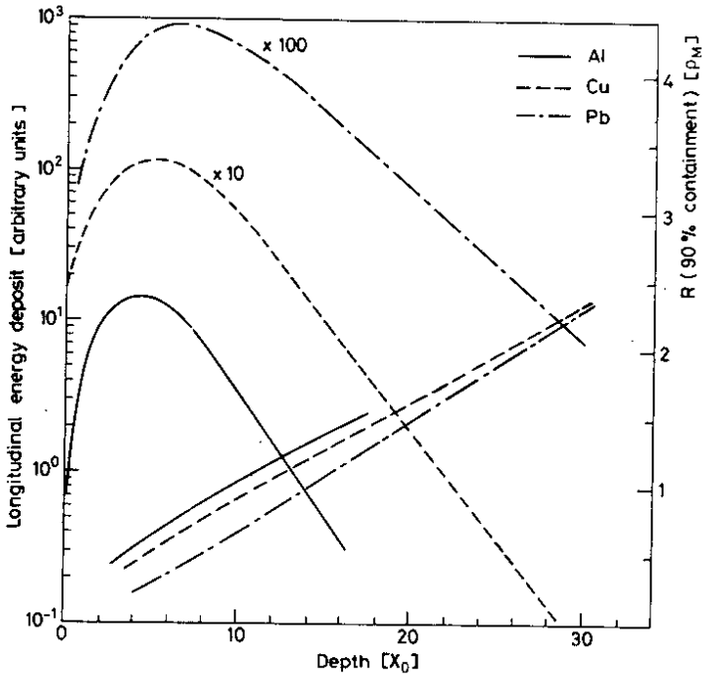

Figure 5 Longitudinal shower development (left ordinate) of 6 GeV/c electrons in three very different materials, showing the scaling in units of radiation lengths X_0. On the right ordinate the shower radius for 90% containment of the shower is given as a function of the shower depth. In the later development of the cascade, the radial shower dimensions scale with the Molière radius $\rho_M \sim 7A/Z$ (data adapted from Bathow et al 1970).

occurs (ε is defined as the energy at which the rate of energy loss per radiation length equals the total energy of the electron). The depth of containment of the shower depends logarithmically on energy. The lateral distribution of the secondaries shows a marked dependence on the depth along the shower axis (Figure 5). Close to the shower maximum, the swarm of still rather energetic secondaries is quite collimated and contained in a cylinder with radius $R_{max} \simeq 1X_0$ deeper in the cascade, the distribution is dominated by multiple scattering of low-energy electrons, which no longer radiate and which travel far from the shower axis. For this part of the shower, the lateral distribution scales in units of the "Molière" radius ρ_M.

Some of the characteristic features of electromagnetic showers are conveniently described in analytic form using "Rossi's approximation B" (Rossi 1964). In this one-dimensional treatment (multiple scattering is ignored), the energy loss of electrons is $\Delta E = \varepsilon/X_0 \simeq 3Z/A$ [MeV g^{-1} cm^{-2}], and the interaction of the secondaries of all energies are approximated by their asymptotic expressions. Under these assumptions the shower distributions in different materials scale in units of X_0 and ε. The total track length T, which is the sum of all track segments of charged tracks, is given in units of radiation lengths, as $T/X_0 \approx E/\varepsilon$. The measurable value T_m of the total track length T depends on the minimum detectable energy η in the calorimeter, and one finds that T_m can be expressed with a universal function $F(\eta$ in the form $T_m = F(\eta) \cdot E/\varepsilon$ (see, for example, Amaldi 1981). Calorimetry works because T_m is also proportional to the incident energy. Furthermore, statistical fluctuations $\sigma(T_m)$ of the measurable track length are found to give the intrinsic limitation to the energy resolution $\sigma(E)$ (see discussion in Section 4).

A striking display of the energy profile of a high-energy electromagnetic shower is presented in Figure 6 (private communication, Sergiampietri 1981).

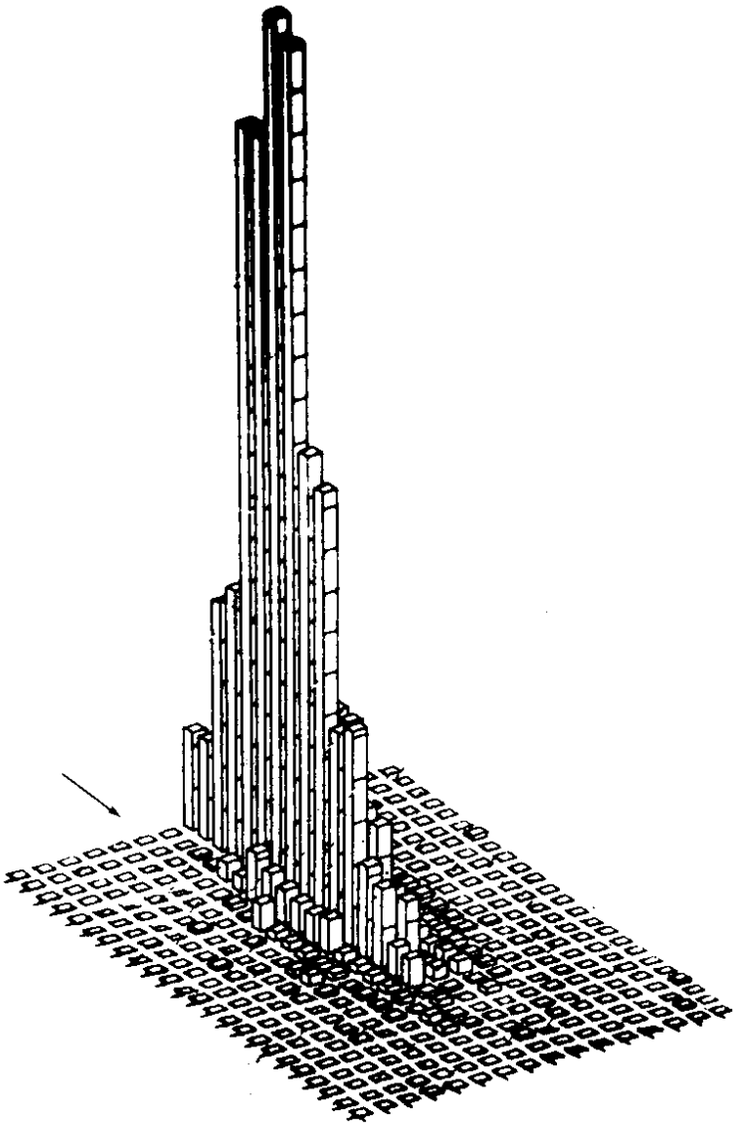

Figure 6 Two-dimensional measurement of an electromagnetic shower induced by a 27 GeV/c electron. The beam direction is indicated by the arrow. The calorimeter is an essentially homogeneous detector of liquid argon. The very fine transverse ($\sim 1X_0$) and longitudinal ($\sim 1X_0$) granularity was achieved with a suitable geometry of charge collecting electrodes (courtesy P. Sergiampietri, Pisa).

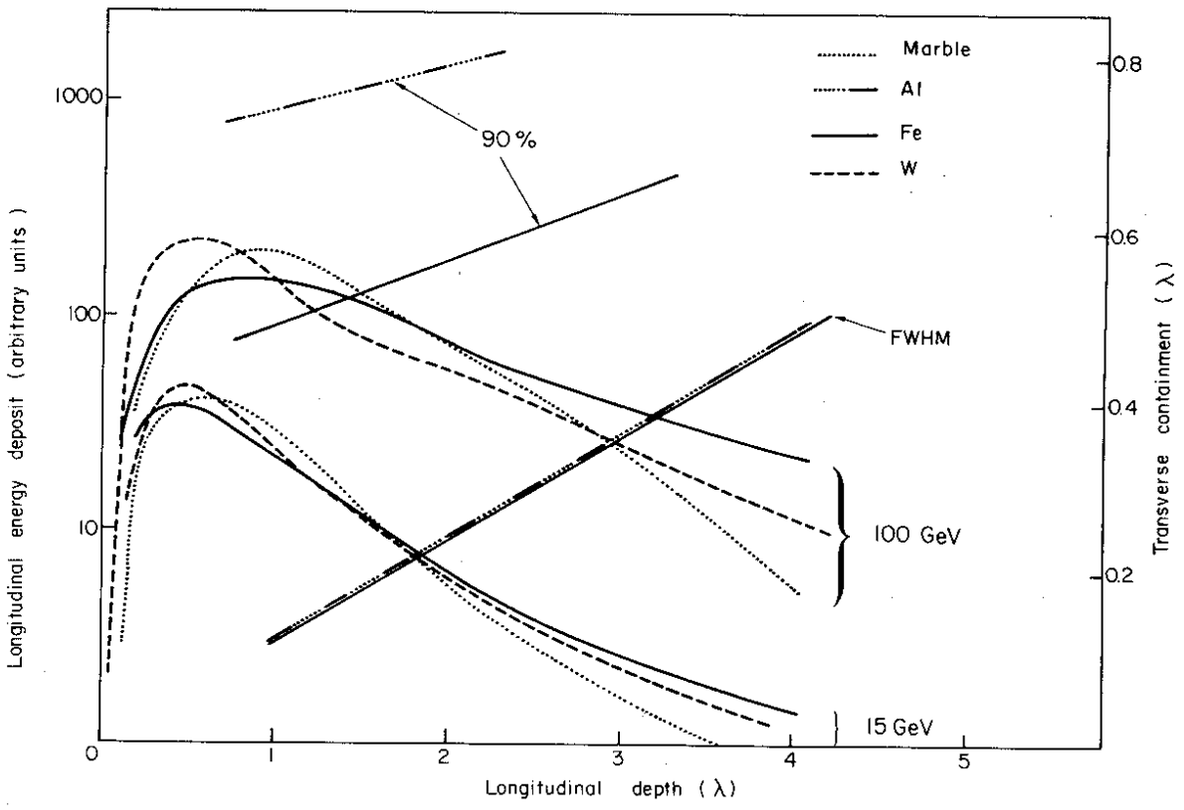

Figure 7 Longitudinal shower development (left ordinate) induced by hadrons in three different materials, showing approximate scaling in absorption length λ. The shower distributions are measured from the vertex of the shower and are therefore more peaked than those measured with respect to the face of the calorimeter. For the transverse distributions as a function of shower depth, scaling in λ is found for the narrow core (FWHM) of the showers. The radius of the cylinder for 90% lateral containment is much larger and does not scale in λ (10 GeV/c π's; Friend et al 1976). Note that marble and aluminum have almost identical absorption and radiation length (Marble: Jonker et al 1982; Al: Friend et al 1976; Fe: Holder et al 1978; W: Cheshire et al 1977).

Table 4 Characteristic stages of hadronic showers

Reaction product	Characteristic time (ns)	Characteristic properties	Effects on energy resolution
Secondary hadrons	$\sim 10^{-22}$	Multiplicity $\sim A^{0.1} \ln E$ [GeV]	Fluctuations in $\pi^{\pm}$ versus π^0 production
Nuclear excitation	10^{-18}–10^{-13}	Emission of p's and n's ($\sim$ 100 MeV); "evaporation" of n's, γ's ($\sim$ 10 MeV)	$\sim$ 15% of hadronic cascade energy converted into nuclear binding energy losses. Large fluctuations and vastly different detection efficiencies.
Pion and muon decay	10^{-8}–10^{-6}	Fractional "invisible" energy $\sim 0.04/\ln E$ [GeV]	Negligible contribution due to small loss of μ's and ν's.

The description of *showers induced by strongly* interacting particles is considerably more complex: a wide spectrum of secondary particles is produced, and nuclear physics effects associated with the excitation of the absorber nuclei are so large that they may dominate effects due to technical features of the detector. The *average* properties of hadronic showers can be parametrized as shown in Table 3, with the characteristic dimensions determined by the nuclear absorption length λ. Examples of longitudinal and transverse distributions are given in Figure 7.

Typical of hadronic interactions is the multiple particle production with limited transverse momentum, $\langle p_T \rangle \approx 0.35$ GeV/c, for which about half of the incident energy is consumed (the inelasticity $\kappa \approx 0.5$). The remainder of the energy is carried by fast forward-going (leading) particles. The secondaries are mostly pions and nucleons, with a multiplicity composition only weakly energy-dependent above the resonance region ($E \gtrsim 1$ GeV). Two features specific to the propagation of hadronic showers constitute the principal limitations to hadronic calorimeters (Table 4):

a) A major component of the secondaries are π^0's, which will propagate electromagnetically without any further nuclear interactions; the average fraction converted into π^0's is $f_{\pi_0} \simeq 0.1 \ln E[GeV]$. The fluctuations in π^0 production from one cascade to the next are mostly determined by the nature of the first inelastic interaction. They are therefore large and approximately at the 50% level.

b) In the hadronic interactions of the cascade, a sizeable amount of the available energy is converted into excitation or break-up of the nuclei, of which only a fraction will eventually appear as detectable energy (see Table 4) with concomitant large event-to-event fluctuations.

Clearly, processes *(a)* and *(b)* are strongly correlated, and together they represent the intrinsic limit to the performance of hadronic calorimeters (Fabjan et al 1975, Fabjan &Willis 1975).

3.2 Calculational Techniques

Detailed understanding of the shower development in various materials, and their dependence on the nature and energy of the incident particle, is essential to the design of calorimeters and the development of improved detector techniques. For these purposes, analytical parametrizations of the average shower behaviour are generally not sufficient, since the most critical measures of calorimeter performance — the resolving power for energy and position measurements — are dictated by event-to-event fluctuations in the shower cascade. For this reason the simulation of showers by Monte Carlo techniques has been developed. In these calculations, which generally have their origins in programs developed to study radiation shielding questions, stochastic models for the elementary electromagnetic and hadronic scattering processes are employed to generate individual cascades and to follow their progress in considerable detail.

Needless to say, the reliability of these results depends on the fidelity of the models for primordial interactions, and on the quality of available data for atomic and nuclear structure of absorber materials. Widely used programs become increasingly predictive as they are refined and checked against measurements. This is particularly true for electromagnetic showers, for which a very general and well-documented system of computer codes called EGS (Electron Gamma Shower) (Ford & Nelson 1978) has been almost universally adopted.

With EGS, one may specify an arbitrary detector geometry; each shower particle is transported, in small steps, through the absorbing media, using cross-sections and branching ratios for the various energy loss processes (Compton scattering, pair-production, and photoelectric effect for photons; multiple Coulomb scattering, annihilation, Bhabha scattering, Møller scattering, and bremsstrahlung for electrons and positrons). The complete history of each generated cascade is available for further analysis, including the energy deposited by individual shower particles in each volume element of material.

One example, showing the detailed agreement with measured data, is given in Figure 8.

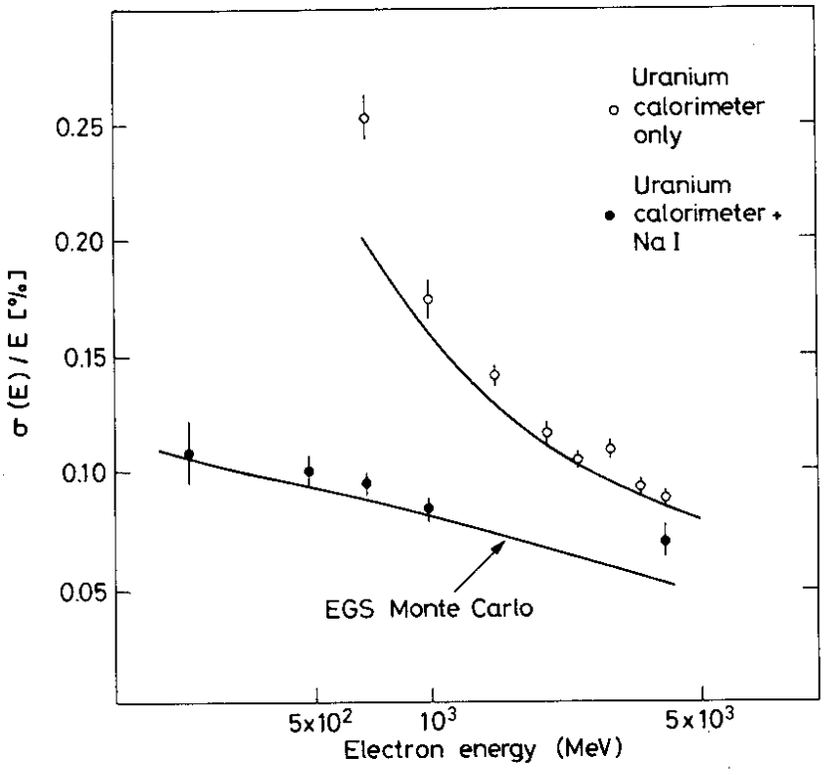

Figure 8 Comparison of measured energy resolution with EGS-Monte Carlo evaluation (solid lines). The high-resolution device consists of $6X_0$ deep NaI crystals, backed up by the AFS hadron calorimeter. The open circles give the energy resolution measured in the uranium calorimeter alone (Jeffreys & Jensen 1982).

The simulation of hadronic cascades is much more complicated. Many approximations are necessary, which must be tailored to the specific application. The principal difficulty stems from a lack of experimental data on the energy-dependent interaction cross-sections for all the different secondary particles. The details of the nuclear break-up, evaporation, and de-excitation must be accounted for, as well as the different response of the active detector medium to the different particles.

A number of hadron shower calculations appear in the literature (Jones 1969, Ranft 1972, Goebel et al 1973, Gabriel & Amburgey 1974, Baroncelli 1974, Grant 1975, Gabriel & Schmidt 1976, Gabriel 1978). Usually these agree well with the average behaviour of experimental data, but often differ in the relative contributions of different energy loss mechanisms, particularly for high-energy (> 10 GeV) showers (Figure 9).

Figure 10 shows a computer simulation of a 100 GeV π^- meson incident on a block of iron and illustrates the large fluctuations in the spatial development of hadronic showers.

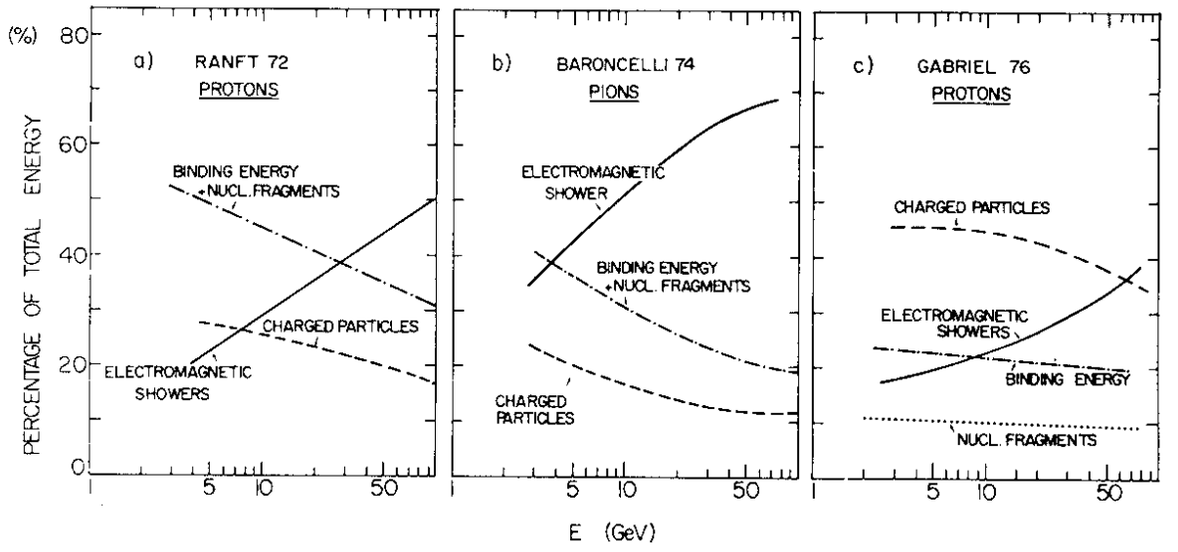

Figure 9 Relative contributions of the most important processes to the energy dissipated by hadronic showers, as evaluated by three representative Monte Carlo calculations (from Amaldi 1981).

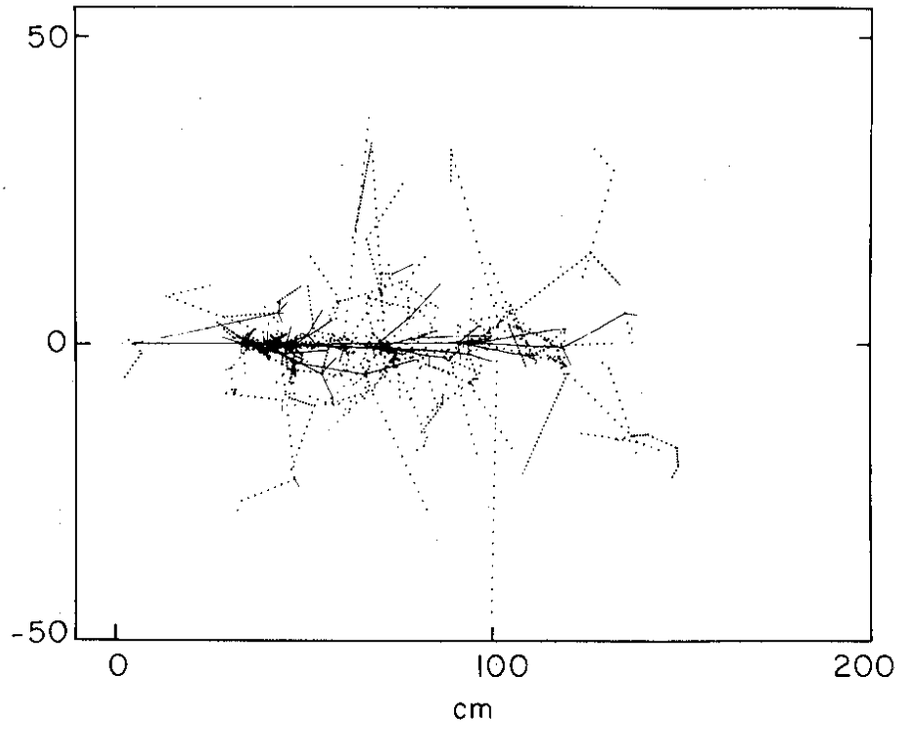

Figure 10 Computer simulation of a hadronic cascade induced by a 100 GeV/c π^- in iron. The dotted tracks represent neutrons which are seen to propagate far away from the shower axis (Grant 1975).

A practical limitation to the use of such Monte Carlo techniques is the necessary computer time. Even the existing limited programs are very costly and become more so in proportion with the shower energy. This is particularly troublesome, because frequently large numbers of showers need to be generated to examine effects in the tails of statistical distributions.

As an alternative to such studies, the considerable body of existing shower data is used to develop parametric approximations to the differential energy deposit over the volume of the cascade. One example for such a parametrization is (Böck et al 1981)

$$dE = k[wt^{a-t}e^{-bt} + (1-w)\ell^{c-1}e^{-d\ell}]\,ds,$$

where t is the depth, starting from the shower origin, in radiation lengths, and ℓ is the same depth in units of absorption lengths. The parameters a, b, c, d are fits to the data, and are given a logarithmic energy dependence. Crude shower fluctuations are simulated by i) randomly varying the depth of the shower origin; ii) smearing the incident particle energy (to simulate the energy resolution of the calorimeter); iii) randomly varying the length of the shower by scaling the values of t and ℓ.

This approach, while obviously not satisfactory for evaluating basic questions of energy resolution, can be very effective for investigating spatial resolution and for studying problems of pattern recognition in multiparticle events, jet reconstruction, etc. (Della Negra 1981, Gordon et al 1981).

4. ELEMENTS OF DETECTOR DESIGN

While the primary goal in designing a calorimeter is usually to achieve the best possible energy resolution for the particles of interest, this is not the sole consideration. Specific experiments generally impose additional requirements. For instance:

- the necessity to cover a large solid angle may render the best techniques prohibitively expensive;
- in large detector systems, particularly for colliding beam experiments, the calorimeter must be tightly integrated with other types of detectors; it may have to function in the presence of strong magnetic fields;
- the necessity to sustain high particle rates or the use of the calorimeter information in fast trigger decisions requires special consideration;
- the degree to which the calorimeter is to be exploited for position measurement and particle identification profoundly influences the nature and complexity of its structure.

In this section we discuss the detector parameters which have a bearing on these issues.

4.1 Energy Resolution

The ultimate limit for the energy resolution of a homogeneously sensitive calorimeter is determined by fluctuations intrinsic to the mechanisms for the development of showers, as described in Section 3. For electromagnetic showers, this limitation results from variations in the net track length of charged particles in the cascade. For hadron showers, fluctuations in the fractional energy loss accounted for by each of several interaction mechanisms set a much higher limit. In both cases, however, the underlying phenomena are statistical processes, whose effects grow in magnitude as $\sqrt{E}$. Hence the limiting accuracy, expressed as a fraction of the total energy, *improves* with increasing energy as $E^{-1/2}$.

In Table 5 we list the major contributions to the final resolution of practical detectors. For electromagnetic showers the intrinsic fluctuations set a limit so small as to be seldom approached in practice. (Indeed, the value given in the table is derived from calculations, not measurements; see Longo & Sestili 1975.)

The most precise electromagnetic measurements are achieved with homogeneous shower counters, in which the entire volume responds with a measurable signal to the passage of charged particles. One such detector with excellent performance is sodium iodide (NaI), a high-density scintillator, with which resolutions close to the shower fluctuation limit have been obtained for energies of $\simeq$ 1 GeV. However, over most of the energy range explored in high-energy physics above 1 GeV, the measurement of electromagnetic showers in this and other detectors is dominated by various instrumental limitations.

This is not the case for hadron showers, as Table 5 indicates. Here the inherent shower fluctuations are the major determinant of the final performance. For this reason there is little practical motivation to employ homogeneous detectors for such measurements. Given the high cost of dense scintillating material and the present highly developed techniques of sampling calorimetry, it is mostly the latter approach that is used for the measurement of hadron showers.

With sampling calorimeters, the shower is developed mainly in an inert absorber material interspersed with an active medium which samples the energy loss at fixed intervals as the cascade develops through the depth of the calorimeter. The typical configuration is a stack of many thick plates of a dense metallic absorber interleaved with layers of active material. The sampled energy measures the ionization loss of shower particles entering the active layers, representing a small but (on the average) fixed fraction of the total cascade. Such constructions are less costly than homogeneous detectors. In addition, one gains the flexibility to optimize the energy and position measurement capability for specific applications, by decoupling the absorber and readout functions. Typical choices for the sampling layers are: plastic scintillators; liquid argon (with the metal absorber plates acting as electrodes of an ion

Table 5 Limitations to energy resolution

Contributing mechanisms (add in quadrature)	Electromagnetic showers	Hadronic showers
Intrinsic shower fluctuations	Track length fluctuations: $\sigma/E \simeq 0.005/\sqrt{E\,[GeV]}$	Fluctuations in the mechanism of energy loss: $\sigma/E \simeq 0.50/\sqrt{E\,[GeV]}$; With compensation for nuclear effects: $\sigma/E \simeq 0.20/\sqrt{E\,[GeV]}$
Sampling fluctuations [a]	$\sigma/E \simeq 0.04\sqrt{\Delta E/E}$	$\sigma/E \simeq 0.09\sqrt{\Delta E/E}$
Instrumental effects	Noise and pedestal width: $\sigma/E \sim 1/E$ – determine minimum detectable signal; – limit low-energy performance. Calibration errors; non-uniformities: $\sigma/E \sim$ constant – limit high-energy performance.	
Incomplete containment of shower (energy leakage)	$\sigma/E \sim \log E$ For leakage fraction $\gtrsim$ few %: non-linear response and non-Gaussian "tail".	

a ΔE = energy loss by a single charged particle in one sampling layer, measured in MeV; E = total energy, measured in GeV.

chamber); and multiwire proportional planes (the active medium being a gas, usually at atmospheric pressure). A detailed discussion of readout techniques is given in Section 5.

For electromagnetic showers in a well-designed sampling calorimeter, the largest contribution to the energy resolution is given by statistical fluctuations in the sampling process, as determined by the energy loss of shower electrons in the sampling layers and, ultimately, by the number of photons or ionization events detected by the readout system.

To first order the sampling fluctuations are determined by the number of sampled electrons n_e in the shower: $\sigma/E \approx 1/\sqrt{n_e}$. In Rossi's "Approximation B", $n_e = E/\Delta E$, where ΔE is the energy loss of a single charged particle in one layer of the calorimeter. For a sampling layer of thickness Δx, one has (cf. Section 2): $\Delta E = (\varepsilon \Delta x/X_0)$ and therefore

$$\sigma/E \simeq \sqrt{\varepsilon} \cdot t/E\,,$$

where t is the thickness of each sampling layer, in units of radiation lengths.

This dependence on the sampling interval and the energy is a well-established characteristic of electromagnetic shower measurements with sampling calorimeters. A more refined parametrization (Amaldi 1981), which is quite accurate for dense (i.e. non-gaseous) sampling materials, is

$$\sigma/E = 3.2\%\,(\varepsilon[MeV]/F(Z)\langle\cos\theta\rangle)^{1/2}(t/E[GeV])^{1/2}$$
$$= 3.2\%\,(\Delta E[MeV]/E[GeV])^{1/2}(F[Z]\,\langle\cos\theta\rangle)^{-1/2}\,.$$

Values for $F[Z]^{-1/2}$ and $\langle\cos\theta\rangle^{-1/2}$ are typically in the range of 1.0 to 1.25. The factor F[Z] accounts for the shortening of the path length due to electrons slowing down and stopping in the sampling medium; $\langle\cos\theta\rangle$ is the mean angular spread of cascade particles about the shower axis.

Some measured values of the resolution for several calorimeter structures are shown in Figure 11. The results with dense sampling media are well described by the above parametrization, while the gas sampling devices give performance figures which are poorer by about a factor of 2. The additional factors which broaden the resolution in the gas-sampling case are related to the signal collection properties in very thin sampling media — a matter which we shall take up in Section 5.

As indicated in Table 5, the energy resolution for hadrons is not determined by sampling fluctuations. These have been measured for hadronic showers (Fabjan et al 1977) and, for a given sampling geometry ΔE, are roughly twice as large as those observed in electromagnetic showers. The dominant contribution to the resolution width comes from fluctuations in the nuclear processes and the correlated loss in detectable energy due to nuclear binding effects, and from the production of particles whose energy goes undetected in the sampling medium. The effect of this invisible

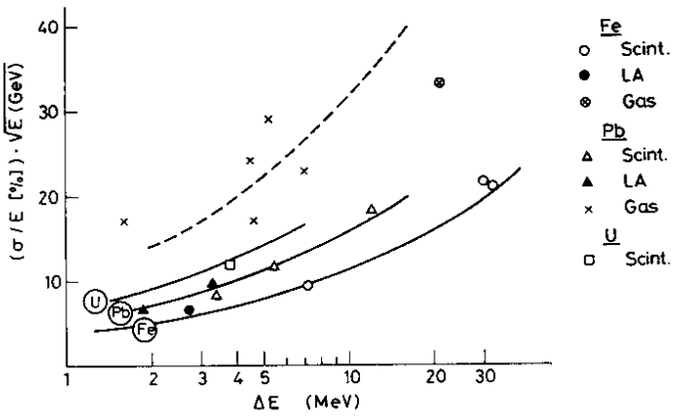

Figure 11 Measured values of the energy resolution for electrons with sampling calorimeters of different constructions: Fe/scint. (Stone et al 1978, Abramowicz et al 1981); Fe/LAr (Hitlin et al 1976); Pb/scint. (Stone et al 1978); Pb/LAr (Hitlin et al 1976, Asano et al 1980); U/scint. (Botner 1981); Pb/gas (Mueller et al 1981, Price & Ambats 1981, Atač et al 1981a, Anderson et al 1978); Fe/gas (Ludlam et al 1981). ΔE is the energy loss in a single sample for a minimum ionizing particle. The solid curves are estimates based on the equation for the energy resolution given in Section 4.1 for the indicated materials and geometries. The dashed curve gives twice the predicted value, representative of the performance of gas-sampling devices.

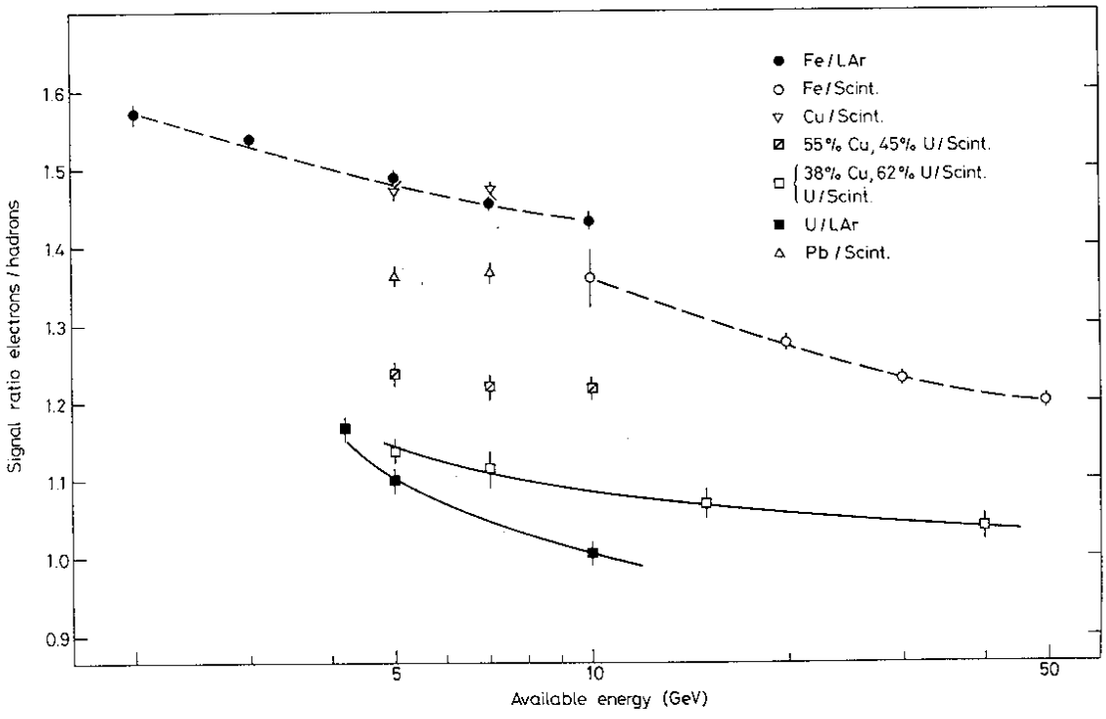

Figure 12 Ratio of average energy deposit for electrons and hadrons as a function of available energy in various materials. The lines through some of the data are drawn to guide the eye (Fe/LAr; U/LAr: Fabjan et al 1977. Fe/scint.: Abramowicz et al 1981. U/Cu/scint.: Botner et al 1981a. Other data: Botner 1981).

energy is clearly seen in the response of a calorimeter to electron and hadron beams (Figure 12). On the average, the ratio of detected signals for electrons/hadrons is $S_{e/h} \simeq 1.4$. Unless event-to-event fluctuations in the electromagnetic component of hadron cascades are somehow corrected for or compensated, the resolution for hadrons is (Table 5):

$$\sigma/E \simeq [(0.5/\sqrt{E})^2 + (0.09\sqrt{\Delta E/E})^2]^{1/2}.$$

If the calorimeter is instrumented so that the signal from each sampling layer is separately recorded to provide detailed longitudinal shower information (as, for example, in the neutrino detectors described in Sec tion 2), then some compensation for the electromagnetic/hadronic fluctuations on a shower-by-shower basis is possible. Relative improvements of about 20% in the resolution for hadronic energies have been obtained by application of weighting procedures based on observed correlations between the total shower signal and the maximum single-layer signal (Rishan 1979, Selove et al 1980, Abramowicz et al 1981).

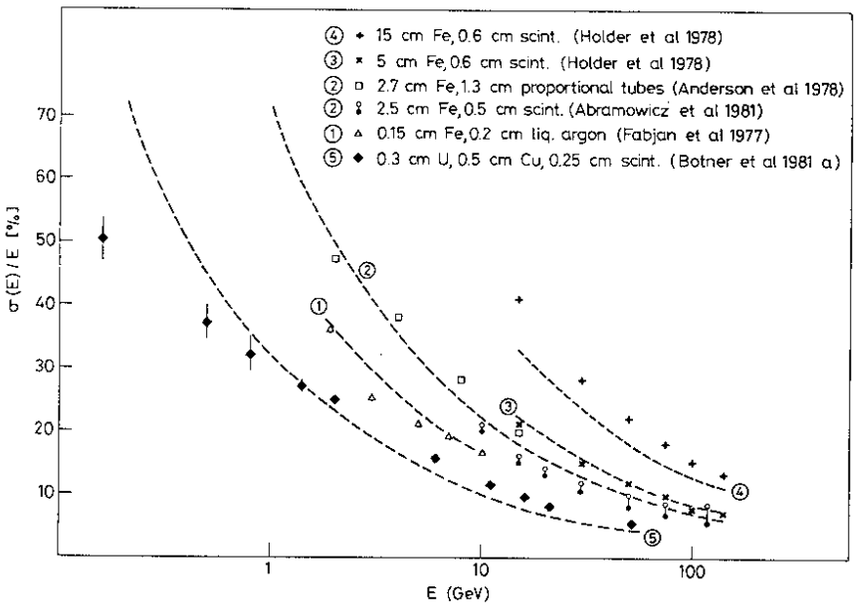

Figure 13 Energy resolution for hadrons measured with iron and uranium sampling calorimeters. Curves 1–4 are calculated with the values for intrinsic and sampling fluctuations as given in Table 5. For the data of Abramowicz et al (1981), the open circles are the raw data; the solid circles are the results of the off-line analysis, using the longitudinal shower information to correct for fluctuations in the electromagnetic/hadronic energy ratio. For curve 5 the intrinsic fluctuation is assumed to be $0.2/\sqrt{E}$, and does not take account of the 35% [in units of λ] admixture of Cu. Below 1 GeV the resolution improves over the expected value and indicates the influence of mechanisms such as ranging and reduced nuclear effects.

A more direct method for improving the energy resolution of hadronic calorimeters by correcting the nuclear fluctuations is based on the use of ^{238}U as absorber material (Fabjan & Willis 1975, Fabjan et al 1977). In the uranium absorber some of the normally invisible energy expended in nuclear break-up leads to neutron-induced fission, which in turn produces detectable energy in the calorimeter, mostly in the form of photons of typically 10 MeV. This mechanism of fission compensation for the unseen energy in nuclear cascades is, coincidentally, almost exact: in tests of a uranium/liquid-argon calorimeter with 1.7 mm thick uranium plates (Fabjan et al 1977), the electron/hadron ratio $S_{e/h}$ was measured to be 1.05 (Figure 12) and the measured energy resolution for hadronic showers was $30\%/\sqrt{E}$. The energy resolution obtained with several representative hadron calorimeters is summarized in Figure 13.

The resolution figures determined by intrinsic shower and sampling fluctuations will not be realized if showers are not adequately contained within the calorimeter volume. In any practical detector some average fraction f of the shower energy escapes through the sides (lateral leakage) or back (longitudinal leakage). (For early-developing hadron showers, some energy may be lost through the front face, a phenomenon referred to as albedo.) The fraction f increases logarithmically with energy, and it is found that lateral containment is less critical for the resolution than longitudinal containment (Amaldi 1981). In either case, values of $f \gtrsim$ a few % yield a measurable degradation of performance (Figure 14).

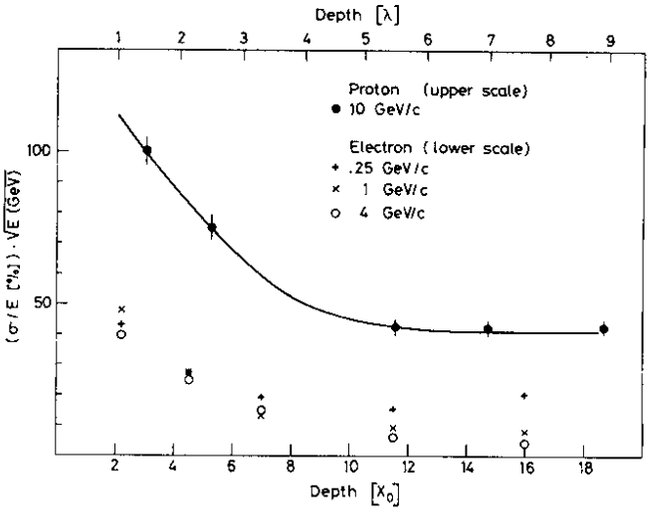

Figure 14 Effect of longitudinal leakage on energy resolution for electromagnetic (Hitlin et al 1976) and hadronic showers (Fabjan et al 1977).

For low-energy showers the resolution may become worse as the calorimeter depth is increased beyond the optimum for containment, owing to larger-than-necessary levels of noise and systematic errors in the readout. This point is illustrated by the measurements shown in Figure 14 (Hitlin et al 1976).

4.2 Position and Angle Measurement: Resolution and Granularity

If the readout is segmented along one or more directions transverse to the shower axis, the location of the shower can be accurately determined by measuring the centroid of the deposited energy. This requires that the transverse cell size be comparable to the lateral shower dimension. For homogeneous detectors this may be achieved by assembling a close-packed array of independent counters. The Crystal Ball detector (Chan et al 1978) is an elegant example of this approach (Figure 15). In sampling calorimeters, the most straightforward Approach is to subdivide the active layers into individually read out strips, with successive layers measuring the position along different coordinates.

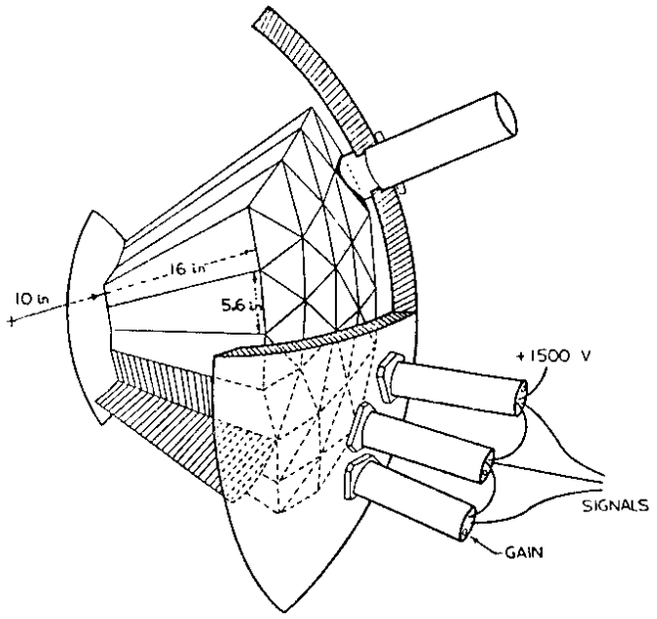

Figure 15 A section of the Crystal Ball detector, containing 54 sodium iodide elements. Each NaI crystal is viewed by a photomultiplier tube, some of which are shown. Almost complete spherical coverage around the e^+e^- collision region is obtained with 672 NaI elements (Chan et al 1978).

For electromagnetic showers, the rms lateral dimension is of the order of a radiation length (typically a few centimeters) and is slowly varying with energy (see Section 3). Spatial resolutions of a few millimeters are achieved for high-energy electromagnetic showers, using lead-glass blocks of lateral dimension $\sim$ 5 cm (Akopdjanov et al 1977, Amendolia et al 1980). Similar resolution values are achieved in sampling calorimeters by subdividing the readout of active layers into 1–2 cm wide segments.

The transverse distribution of hadron showers is approximately one absorption length, substantially broader than for electromagnetic showers, and fluctuations in the distribution of deposited energy through the volume of the cascade are larger. For a calorimeter segmentation s, a spatial resolution $\sigma_x \approx 1.0 \exp(1.2s/\lambda)$ (all dimensions in cm) is obtained (Amendolia et al 1980). Position accuracies $\lesssim 1$ cm can be achieved (Binon et al 1981), but figures of merit of a few centimeters are more typical. The use of shower measurements to determine the direction of the initiating particle has been carefully studied in connection with the large neutrino detectors. For the detector of FNAL experiment 594 (see Table 2) the energy dependence of angular resolution for electrons and hadrons was measured to be $\sigma(\theta_e)$ [mrad] = 3.5 + 53/E[GeV] and $\sigma(\theta_h)$ [mrad] = 6 + 640/E[GeV] (Bogert et al 1981). With the CHARM detector (Figure 1) an angular resolution $\sigma(\theta_h)$ [mrad] = $160/E^{1/2}$[GeV] + 560/E[GeV] was obtained for hadrons and about an eight times better resolution for electrons (Diddens et al 1980). In both cases the angular fluctuations were minimized by choosing an absorber material in which electromagnetic and hadronic showers have approximately equal length ($12X_0$ [cm] $\simeq 3\lambda$ [cm]).

In most applications it is important that the calorimeter be able to measure simultaneously the position and energy of two or more particles, and several important types of calorimetric measurements are limited by the ability to resolve close pairs of showers. One example is the signature of high-energy π^0 particles.

With well-segmented calorimeters, the limit for distinguishing nearby showers is determined by the lateral size and shape of the cascade. Electromagnetic showers can be distinguished down to separations of $\gtrsim 1X_0$ (Kourkoumelis et al 1980). For hadron showers the minimum separation of resolved pairs is $\gtrsim 1\lambda$.

For events with high multiplicities of particles striking the calorimeter, the pattern recognition problem becomes severe if the lateral segmentation is in strips and projections have to be used for the reconstruction of space-points. In present-day colliding beam experiments, the interesting events tend to be just those in which a very large number of particles enter the detectors. While for some measurements it is sufficient to record the angular distribution of particle energies rather coarsely, classifying events in terms of patterns of energy flow, it is more frequently required to measure the energies of individual particles in events of high particle density. In this case it is necessary to segment the readout into cells which are small in both lateral dimensions, as in the Crystal Ball configuration (Figure 15) or in the TASSO shower counters (PETRA Bulletin No. 14, 1979).

An example of the motivation for fine-grained spatial segmentation is shown in Figure 16. This is a simulation (Gordon et al 1981) of an event in which two jets of particles result from the hadronization of a pair of heavy quarks produced in 400 GeV colliding proton beams. Such events are extremely rare and difficult to isolate, yet their detection and measurement is one of the primary reasons for constructing high-energy colliding beam machines. By recording the energy deposited in each of the eight calorimeter modules, one could recognize the presence of the two jets in this event and measure the energy carried by each. But this is not enough. Figure 16b shows the energy deposited in module 3, as seen by a fine-grained readout organized into towers of 20 cm side. With this information it is possible to reconstruct detailed correlations between energy and angle within the jet of particles (e.g. to measure the invariant mass of the jet).

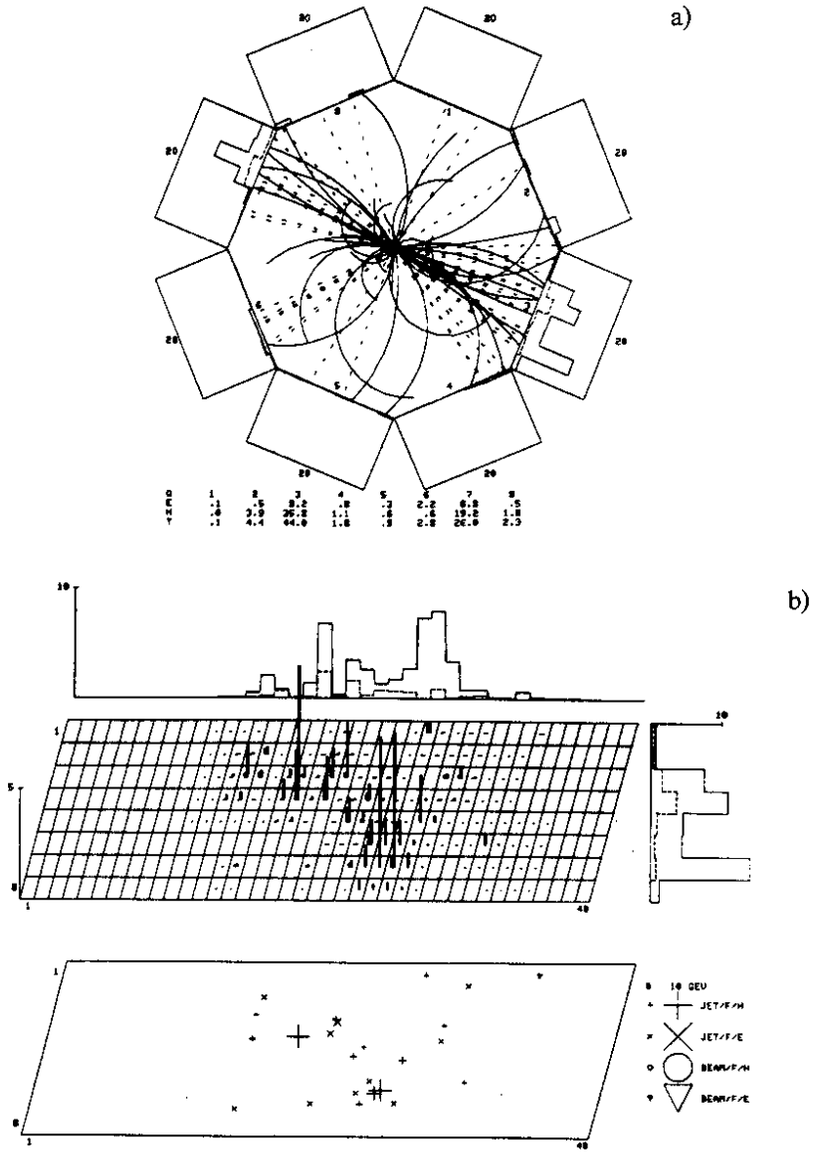

Figure 16 a) Monte Carlo simulation of an event producing high-energy jets of particles in the collision of two 400 GeV/c p beams. Solid trajectories are charged particles in a 1 T magnetic field; neutrals are dashed. The energy deposition in the eight calorimeters is indicated. b) Response of octant 3 for the same event. It is subdivided into 8 × 46 towers of 20 cm side. The signal recorded in each tower, of which the first 10 radiation lengths are read out separately, is indicated by the length of the two bars (energy in GeV with scale on lower left). For comparison the point of impact of the particles is also shown (size of indicator is proportional to energy) (Gordon et al 1981).

4.3 Particle Identification

Such measurements, which are not usually associated with calorimeter applications, have traditionally implied identification of protons, charged pions, and kaons. With the discovery of the "new" quarks, emphasis has shifted to the identification of signatures from c, b, and possibly heavier quarks. Various techniques are applied to these "modern" identification requirements and we summarize here the role of calorimetry. Table 6 gives an overview.

Table 6 Particle identification with calorimeters

Particle produced	Calorimeter technique	Comment
Electron, e	Charged particle initiating the electromagnetic shower	Background from charge exchange $\pi^{\pm}N \rightarrow \pi^0 + X$ in calorimeter; π discrimination of $\sim$ 10–1000 possible
Photon, γ	Neutral particle initiating the electromagnetic shower	Background from photons from meson decays
$\pi^0, \eta, \ldots \rightarrow \gamma\gamma$ $\rho, \phi, J/\psi, Y, \ldots \rightarrow e^+e^-$	Invariant mass obtained from measurement of energy and angle	Classical application for electromagnetic calorimeters;
Protons, deuterons, tritons, ... and their antiparticles	Comparison of visible energy E_{vis} in calorimeter with momentum of particle	$E_{vis}^{b(\bar{b})} = (\vec{p}_b^{\,2} + m_b^2)^{1/2} - (+)\, m_b$ Protons (antiprotons) identified up to 4 (5) GeV/c; deuterons (antideuterons) correspondingly higher
(Anti)neutrino	Visible energy E_{vis} in calorimeter compared with missing momentum	Important tool for $e^+e^- \rightarrow \nu(\bar{\nu}) + X$ and at CERN collider (ISABELLE, ...) $pp(\bar{p}p) \rightarrow \nu(\bar{\nu}) + X$
Muon	E_{vis} compared to $\vec{p}$; range	Background from non-interacting pions
Neutron or $K_L^0(\bar{n}, \bar{K}_L^0)$	Neutral particle initiating hadronic shower	Some discrimination perhaps possible based on detailed (longitudinal) shower information

The art of identifying *electrons* is usually based on a coarse measure of the longitudinal shower profile. Dominant background comes from charged π's producing a leading π^0 system through charge exchange in the calorimeter, with a probability at the percent level for few GeV/c π's. Typically, therefore, a π rejection of about 100 is achieved if information on the momenta of the incident particles is not available, but may approach about 1000 if momentum measurements are included (Apel et al 1975, Lederman et al 1975, Cobb et al 1979, Basile et al 1979). As the charge-exchange cross-section drops with increasing energy, a π rejection factor approaching 10^4 is expected for momenta $p \simeq 100$ GeV/c. The effect of this hadronic background is minimized by building detectors from absorbers with a large ratio of $\lambda/X_0 \sim Z^2/A^{3/4}$. Lead is therefore a popular choice for the electromagnetic part of calorimeters. A further small (about 2 to 3) improvement in rejection is achieved if transverse shower dimensions are measured (Lederman et al 1975, Cobb et al 1979). Longitudinal information on early shower development is provided by the "converter" method. A combination of a $\sim 1X_0$ thick Pb plate followed by a scintillator or a multiwire proportional chamber (MWPC) ("passive" converter) or by instrumented layers of lead-glass Čerenkovs ("active" converter) can signal an early interaction, predominantly of electromagnetic origin (Lederman et al 1975, Gabathuler et al 1978). The ultimate "converter" for relativistic electrons is not based on bremsstrahlung emitted from one X_0 of a high-Z material, but rather exploits radiation emitted from $\sim 0.01X_0$ of very low-Z substances: transition radiation detectors (Cobb et al 1977). These "converters" will be particularly valuable for the identification of electrons amidst densely collimated jets of hadrons (Fabjan et al 1981).

In a similar way, *photons* are identified which are either produced directly (Diakonou et al 1979) or from meson decay. It has been found that a transverse granularity in $2X_0$ allows discrimination between one and two photons (e.g. from π^0 decay) if they are separated by more than one radiation length.

Identification of particles through the determination of the *invariant mass of their decay products* is a rather standard calorimetric method, on which a number of interesting recent physics results were based: charmonium spectroscopy; discovery of the η_c (Coyne 1981) and the hadronic production of χ states (Kourkoumelis et al 1979); the possible detection of a state $\theta(1640) \rightarrow \eta\eta$ (Scharre 1981), considered a glueball candidate; the discovery of directly produced high-p_T photons and their separation from high-p_T π^0's — all illustrate the power of this method and its role in the "new" physics.

An interesting method for identifying *protons, deuterons,* etc., and their *antiparticles* over a limited momentum range is possible through a comparison of the particle's momentum with its characteristic energy deposition, its

"available energy". For electrons and protons this is the kinetic energy of the particle; for mesons, it is the total energy; while for antiprotons it is the total energy plus one proton mass (Fabjan et al 1977, Corden et al 1982). Proton and antiproton identification up to about 4 GeV/c is possible. Hadronic high-p_T production of antibaryons may also be studied, as the increased available energy at a given p_T dominates the $\pi^{\pm}$ trigger rate over a limited kinematical region (Willis 1979, Botner & Fabjan 1981). Recently, the calorimeter response to *nuclei* with A in the range 2 to 20 has been measured and found to be proportional to the kinetic energy (Stevenson et al 1981).

Muon identification with calorimeters is an important technique for neutrino physics and for the detection of uncommon particle decays (charm, W, etc.). In calorimeters with frequent longitudinal subdivision (e.g. neutrino detectors), the multiple ionization measurement consistent with the passage of fast μ's discriminates against pions, which penetrate with a probability exp $(-d/\tilde{\lambda})$. The observed path length d is measured in units of "detectable" absorption length $\tilde{\lambda}$, which is found to agree closely with tabulated values (Baum et al 1975, Grant 1975, Holder et al 1978). With purely passive absorbers, μ's may be separated from π's to a lesser degree, based on their different "punch-through" probability. Spatial consistency between the tracks entering and exiting the absorber within multiple scattering limits enhances the discrimination (Grant 1975). Events containing high-p_T *neutrinos* will probably be studied with a calorimetric technique for the first time at the hadron collider. The method is based on a precise measurement of the missing momentum in an event. It might be comparatively easy for cases such as $W \rightarrow \ell\nu$ decay, where the ν is reflected in the characteristic spectrum of the charged lepton. As already mentioned in Section 2, missing-momentum techniques are expected to find their widest ranging applications at future e^+e^- colliders.

4.4 Rate Capability and Trigger Selection

The event rates at hadron machines, either fixed-target or colliding beams, can be enormously high. The collision rate at the ISR, operating in the luminosity range 10^{31}–10^{32} cm^{-2} s^{-1}, is $\gtrsim 1$ MHz, and luminosities higher by an order of magnitude are contemplated for ISABELLE. The power of these machines is not the high collision rate in itself, but the capability to produce useful numbers of very rare events over periods of months. A very high degree of trigger selectivity is required, rejecting most events seen by the detectors. Indeed, a large detector system with thousands of readout channels generally cannot record more than a few events per second.

The rate and trigger capability depends on the intrinsic resolving time of the calorimeter, which is determined by the time required to develop a measurable signal in the readout medium and by the pulse-shaping time required for noise filtering. If this time is comparable to the mean time between events, then the energy recorded for a particular event will be influenced by "pile-up" of spurious energy deposited by nearby events in time. The typical resolving times for calorimeters range from a few tens of nanoseconds (for scintillator readout) to several hundred nanoseconds (for charge collection readout) (see Section 5).

For most high-energy physics applications, the effect of energy and time resolution on trigger selectivity is intimately coupled with the rapid decrease in the particle production spectrum as a function of the transverse momentum p_T. As an example, we show in Figure 17 the p_T spectrum of incident particles and the result of the measurement, which is distorted by such pile-up effects according to the following assumption: 20% probability for two

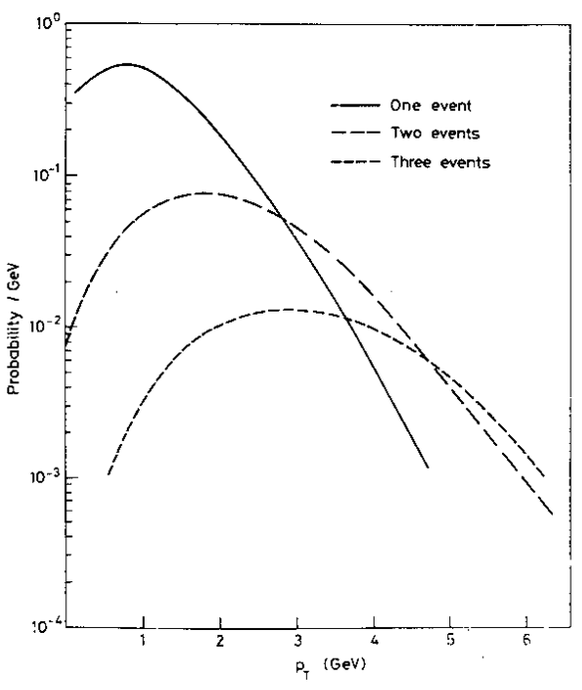

Figure 17 Influence of detector resolving time on the measured transverse momentum spectrum. This example assumes a 20% (4%) probability for two (three) collisions to occur within the resolving time.

events to occur within the resolving time of the calorimeter (and, by Poisson statistics, a 4% probability for three events, etc.). In this case, most of the events above 3 GeV result from multiple event pile-up, depicted by the dashed curves in Figure 17 (Carithers 1982).

Other factors related to high rates include space-charge saturation effects, which may be important in the case of gas sampling with avalanche gain (see Section 5), and limited detector lifetime. Scintillators, lead glass, wire chambers, and the components of sensitive preamplifiers all suffer a measurable degree of radiation damage after integrated particle fluxes $\gtrsim 10^{12}/\text{cm}^2$ (Schönbacher & Witzeling 1979, Hilke 1981).

4.5 Calibration and Monitoring

A large calorimeter consists of many individual detector elements, each of which must be continually and precisely adjusted if the performance of the device is not to be dominated by systematic errors. This usually implies gain control of each analogue readout channel to about 1%.

With the calibration and monitoring scheme, one needs to

a) establish an absolute energy scale;

b) compensate for time variations of the response of individual channels (e.g. thermal drifts);

c) detect malfunctioning channels.

For these purposes a mechanism is required for injecting a known calibration signal into each channel. For lead-glass and scintillation counters this is achieved by distributing precisely controlled pulses of light to each detector element. In large systems it is current practice to illuminate a bundle of optical fibers with a single light-source, each fiber being connected to an individual detector element. Lasers or gas discharge lamps are used as light-sources (Powell et al 1981, Clark 1981).

Alternatively, radioactive sources are used to excite the scintillator. This provides a very stable calibration signal, completely monitoring the active system. Ideally, such sources are uniformly distributed in the calorimeter (Botner et al 1981a) or are permanently introduced into certain areas (Botner et al 1981b), or they are mounted externally for dedicated calibration runs (Corden et al 1982).

For charge collection devices (e.g. liquid-argon and proportional wire calorimeters) a voltage pulse across a fixed capacitor injects a measured calibration charge at the input of each amplifier in the system (Cobb et al 1979).

The absolute energy scale is determined by exposing each detector element to particles of known energy (e.g. monoenergetic electron beams), or known energy deposit (e.g. muons). In fixed-target experiments this step can be accomplished by scanning the calorimeter array across the beam with a system of rails and stepping motors. For colliding beam experiments the initial energy calibration must be done in test beams. Once the detector is in place, an absolute energy scale can be obtained from cosmic-ray muons or, in the case of e^+e^- machines, from elastic (Bhabha) scattering events.

In most experiments a final adjustment of the overall energy scale is made during the later stages of data analysis, using the known masses of reconstructed particles and narrow resonance states (π^0, η, J/ψ, Y, ...).

For today's very large detector systems, the task of injecting calibration pulses into each channel, adjusting voltage settings to compensate for gain changes, and preparing a parameter list for off-line corrections, is done exclusively under computer control (Breidenbach 1981).

We stress that the quality of the calibration system will have the most pronounced influence on the performance of a calorimeter facility. In the conceptual design stage of such a detector, various alternatives must therefore be evaluated in conjunction with a careful assessment of the respective calibration methods.

5. READOUT TECHNIQUES

In the previous sections we discussed the physics and detector requirements of large experimental facilities, as well as the properties of electromagnetic and hadronic showers and their consequences for the performance of calorimeters. Much of the recent calorimeter developments concentrated on instrumental techniques for converting the signature of the showers into a measurable signal, which would be well matched to the experimental requirements. These "readout" techniques are described in this section.

Two different methods have found wide applications and are schematically shown in Figure 18.

1) "Photon collecting" techniques are based on scintillation or Čerenkov light in the active medium. A system of light-guides is usually required, and light is converted into charge with photomultipliers. This technique can be mechanically engineered into large systems with relative ease. However, light collection is intrinsically non-isotropic, light-guides introduce non-uniform areas, and calibration is complex.

2) "Charge collecting" techniques measure the ionization produced in the active absorber; the charge may be amplified with external circuitry ("ionization chamber" mode) or to various degrees internally at the charge collecting electrodes (proportional mode, Geiger mode, etc.). Charge-collection uniformity is good, segmentation and calibration easy.

We first discuss homogeneously sensitive detectors, which offer attractive possibilities for the energy measurement of electromagnetic showers. Next, sampling devices are discussed, which are widely used for electromagnetic calorimetry and offer the only practical method for hadron detectors.

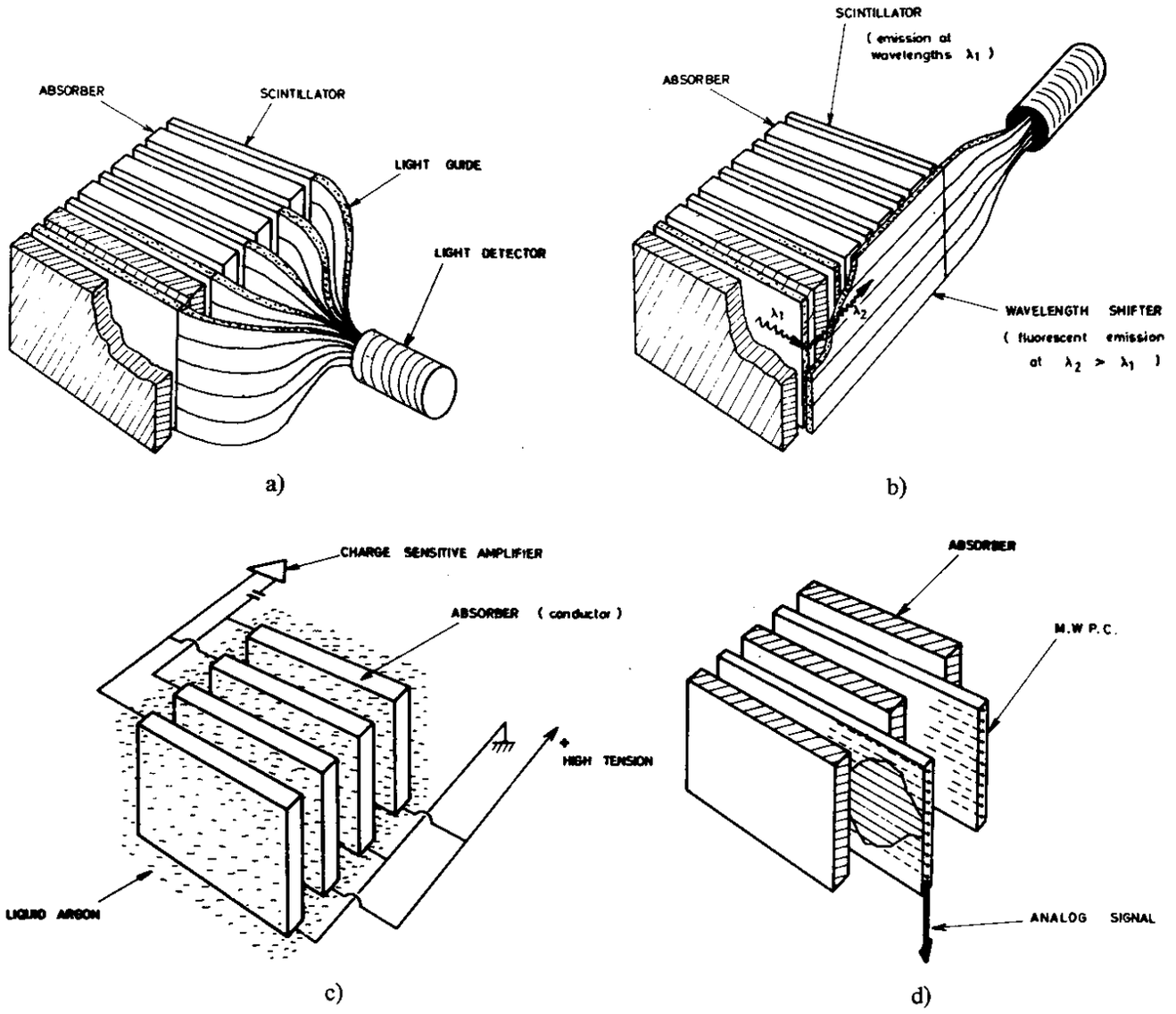

Figure 18 Schematic representation for frequently used calorimeter readout techniques: a) Plates of scintillator optically coupled individually to a photomultiplier. b) Plates of scintillator readout by photon absorption and conversion in a wavelength shifter plate. c) Charge produced in an electron-transporting medium (e.g. liquefied or high-pressure argon) collected at electrodes, which may also function as the passive absorber plates. d) Charge produced in a proportional gas and amplified internally on suitable readout wires (proportional or saturated gas amplification).

5.1 Homogeneous Calorimeters

The intrinsically superior energy resolution for electromagnetic showers is the principal attraction of homogeneous absorbers. Practical detectors may be realized given the relatively small size of electromagnetic showers. For hadronic calorimeters, homogeneous systems offer no interest and would be impractically large.

A summary of homogeneous detector properties is given in Table 7. The following parameters are of primary interest:

- Energy resolution: NaI and BGO show the best performance.
- Short radiation length: this permits compact detectors and very high granularity. BGO is most attractive.
- Light output: it is highest for NaI and permits detection with vacuum photodiodes and external amplifiers. Very compact detectors, insensitive to strong magnetic fields, can be constructed (Anassontzis et al 1981).
- Radiation resistance: lead-glass and scintillators are known to be affected. Helicon appears to be more resistant.
- Mechanical ruggedness: lead-glass and BGO excel.
- Price: for correctly designed detectors the price/X_0^3 is relevant. Expressed in these units, NaI and BGO are rather comparable. Surface treatment of the absorbers is expensive but may be minimized by employing novel production or assembly techniques without significant loss in performance (Grannis et al 1981, Bartalucci et al 1980, Anassontzis et al 1981).

Table 7 Properties and performances of electromagnetic shower detectors

Type	Rad. length (cm) *Density ($g\,cm^{-3}$)*	Detection mechanism	Energy resol. $\sigma(E_{GeV})$	Principal limitation to $\sigma(E)$	Signal (photoel./GeV) *Charact. time (ns)*	Radiation damage (rad)	Mechanical stability	References
Sodium iodide NaI (Tl)	2.59 *3.7*	Scintillation	$\sim 0.015E^{-1/2} < 1$ GeV $\sim 0.015E^{-1/4} > 1$ GeV	Shower fluctuations Optical non-uniformity	10^6 *250*	10^4	Hygroscopic, fragile	Beron et al 1973 Chan et al 1978
Bismuth germanate $Bi_4Ge_3O_{12}$ ("BGO")	1.12 *7.13*	Primary scintillation	Below 1 GeV comparable to NaI	Similar to NaI	$\sim 10^5$ *350*	~ 1000	Good	Blenar et al 1981 Kobayashi et al 1981a
Scintillating glass	~ 4 *~ 3.5*	Scintillation, some Č light	$\sim 0.02E^{-1/2}$	Photon statistics	few $\times 10^3$ *~ 70*	$\sim 10^6$	Good	Yoshimura et al 1976 Kobayashi et al 1981b Bartalucci et al 1980
Lead-glass (55% PbO, 45% SiO_2)	2.36 *4.08*	Čerenkov light	$\sim 0.04E^{-1/2}$	Photon statistics	10^3 *~ 20*	$\sim 10^4$	Good	Bartel et al 1979
Tl (HCO_2)-liquid "Helicon"	~ 1.9 *~ 4.3*	Čerenkov light	Comparable to Pb glass	Photon statistics	$\lesssim 10^3$ (?) *~ 20*	$\gtrsim 10^6$	Liquid, toxic (?)	Kusumegi et al 1981
Liquid argon	14 *1.4*	Ionization charge	$\lesssim 0.02E^{-1/2}$	Effect of shower fluctuation on electron collection	$\lesssim 2 \times 10^6$ (electrons) *$\gtrsim 100$*	Not measured	Cryogenic liquid	Chen et al 1978 Radeka 1977

5.2 Readout Systems for Sampling Calorimeters

5.2.1 LIGHT COLLECTING SAMPLING CALORIMETERS The renaissance of such calorimeters started with the introduction of cheap "plastic scintillators" and elegant light-readout techniques using "wavelength shifters" (WLSs), replacing the cumbersome scheme of scintillator plates individually coupled to a light-guide (Figure 18a). The principle is indicated in Figure 18b (Garwin 1960, Erwin et al 1975, Selove et al 1979, Botner et al 1981a). Some scintillation light crosses an air gap and enters the WLS, where it is absorbed and subsequently re-emitted at longer wavelengths; a fraction of this "wavelength shifted" light is then internally reflected to the light detector. This scheme avoids complicated and costly optical contacts between the scintillators and light collectors, and minimizes dead spaces. A variety of scintillators have been developed for the large calorimeter facilities. They are based on "PMMA" (polymethyl methacrylate) (Kienzle 1975) or polystyrene (Corden et al 1982) as the matrix for the primary scintillating agent. The light yield is close to that of more conventional organic scintillators (usually based on a polyvinyl toluene solvent), if certain aromatic compounds, e.g. up to about 20% naphthalene, are added. These new scintillators are more easily mass produced, hence cheaper, and have superior mechanical properties. Some of the limitations of the WLS method may be removed by further developments: better spectral matching between the scintillator emission and the WLS absorption, and also between the WLS emission and the photocathode sensitivity will increase the number of detected photons, which is marginal in present systems. Related developments might result in the use of thinner yet more uniform WLSs; increased granularity might be achieved with WLSs having spatially different spectral sensitivities (Eckardt et al 1978). Potentially the most promising developments concern scintillators: they are still rather inefficient (a few percent of the energy loss is converted into visible photons), and reduced saturation of the response to densely ionizing nuclear fragments should improve the energy resolution of hadron calorimeters (see Section 4). This is an important scintillator property for calorimeter applications and it should be carefully investigated and specified.

5.2.2 CHARGE COLLECTION READOUT The ionization charge produced from the passage of the charged particles of the shower may be collected from solids, liquids, or gases. Solids (Brisson et al 1981) and liquids can only be used in an ionization chamber mode with no internal amplification. The best known and to date only practical example is based on the use of liquid argon (Willis & Radeka 1974). In specific cases, liquid xenon may be used (Alvarez 1968, Derenzo et al 1974, Masuda et al 1980, Doke 1981). The use of room-temperature liquids has also been advocated (private communication, Gruhn 1974), but with increasing operating temperature the tolerable level of impurities decreases strongly: for liquid-argon operation, impurity concentrations at the ppm level are acceptable; liquid-xenon operation requires control close to the ppb level; while for room-temperature operation, even lower values are required. If gas is used as the active sampling medium, internal amplification to various degrees is usually exploited: proportional chambers or tubes provide a signal proportional to the energy loss. At higher gas gain, with devices operating in a controlled streamer or Geiger mode, the measured signal is related to the number of shower particles which traverse the active medium ("digital readout") (Conversi 1973).

The principal advantage common to all these charge collection methods is seen in the ease of segmentation of the readout and the capability to operate in magnetic fields.

Some features specific to the various types are:

a) operation in the ionization mode, i.e. liquid-argon calorimeters provide the best energy resolution and control of systematic effects (cf. Figure 11) (Cobb et al 1979, Davies-White et al 1979, Kadansky et al 1981, Behrend et al 1981, Slattery et al 1981);

b) gas proportional devices offer a wide variety of relatively inexpensive construction methods (Anderson et al 1978, Bosio et al 1978, Stone 1981);

c) digital operation, in the Geiger or streamer mode, allows for very simple and cheap signal-processing electronics (Conversi & Federici 1978, Walker et al 1981, Jonker et al 1981).

For ion chambers and proportional wire readout the measured signal amounts to a few picocoulombs of charge per GeV of shower energy. Since sampling calorimeters are inherently devices of large capacitance, the optimum charge measurement requires careful consideration of the relationships between signal, noise, resolving time, and detector size. A detailed noise analysis gives (Willis & Radeka 1974)

$$\mathrm{ENC_{opt}} = 5.9 \times 10^6 (\mathrm{C_D}[\mu\mathrm{F}]/\mathrm{t_{NF}}[\mathrm{ns}])^{1/2}$$

(ENC "equivalent noise charge", is the input signal level which gives the same output as noise; C_D is the detector capacitance, and t_{NF} is the noise filter time). This result gives the fundamental lower limit to the noise, achieved with optimal capacitance matching between the detector and amplifier. The noise figure grows with increasing detector capacitance and can be improved at the expense of increasing resolving time.

Some general features of proportional charge collection devices are illustrated in Figure 19 for two model detectors, each with parameters typical of its type: a liquid-argon calorimeter with ion chamber readout, and a gas sampling calorimeter with multiwire proportional planes for the readout. For each case the absorber layers are 2 mm lead sheets, with sampling geometries which give good energy resolution. For the ion chamber, the measured charge is induced on the collecting electrode by the drifting electrons, and amounts to 50% of the total ionization charge (Rossi & Staub 1949). In the case of proportional wires, the observed signal is due to the motion of positive ions away from the

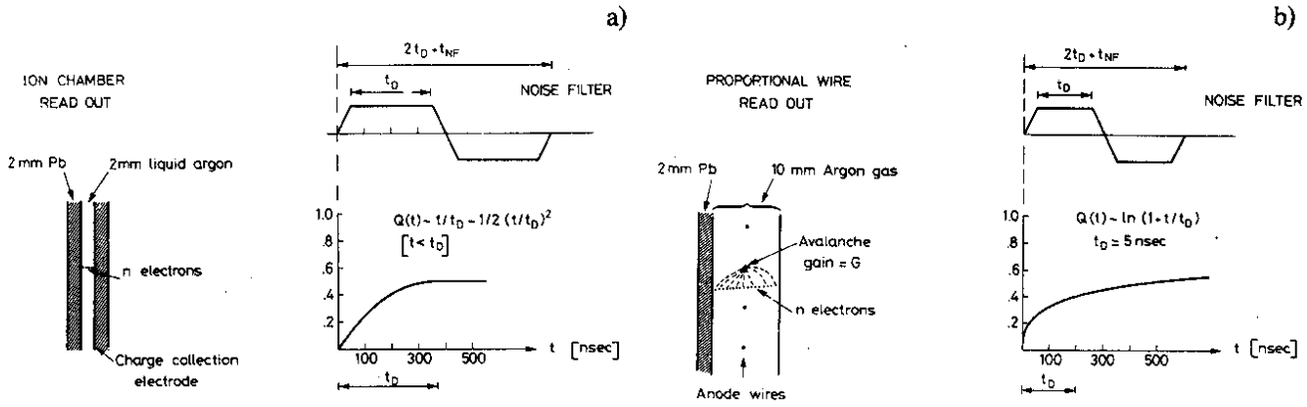

Figure 19 Charge collection in a single sampling layer for a) liquid argon calorimeter with ion chamber readout; b) gas proportional wire readout. The signal charge Q(t) is shown as a function of time, and t_D is the time required for all ionization electrons to be collected. For each case a bipolar noise filter weighting function is indicated (see text).

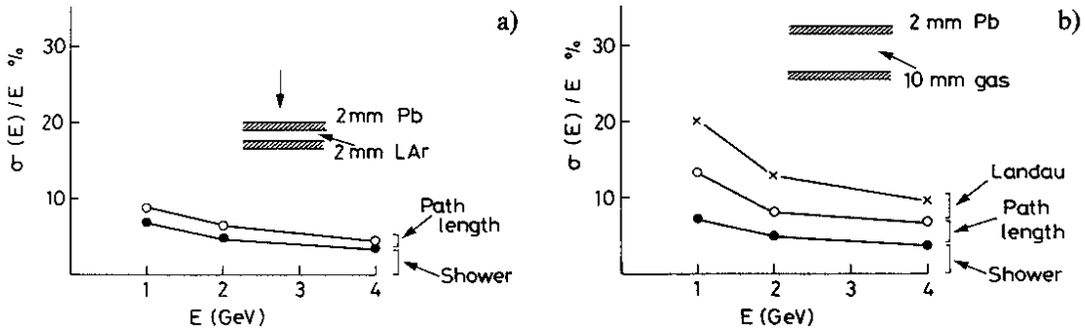

Figure 20 Calculated energy resolution, with electrons at normal incidence, for the two model calorimeters (see text and Figure 19). The lowest curve includes only the effects of fluctuations in shower development, the next curve includes both shower and path length fluctuations, etc. Landau fluctuations contribute negligibly in the liquid argon case.

anode wire (Sauli 1977), with about 30% of the total charge collected during the rapidly developing early part of the signal. In both examples a bipolar pulse-shaping wave form is indicated, with noise filter time $t_{NF} \simeq 100$ ns. Possible trade-offs between resolving time and noise are exploited more freely in gas sampling calorimeters, where there is some freedom in the choice of avalanche gain and the inherently poorer resolution reduces the sensitivity to noise. The noise penalty can be severe for very large calorimeters which must sustain high particle fluxes (Radeka & Williams 1981).

Energy resolution curves for the two model calorimeters of our illustration are shown in Figure 20 for electromagnetic showers. These Monte Carlo calculations agree well with measured results from real detectors of similar specification. For the liquid-argon detector the resolution is dominated by statistical fluctuations in the number of sampled shower electrons. The remaining component is mainly due to variations in the path length of electrons traversing the sampling gap: soft shower electrons are brought to rest depositing all their kinetic energy in the sampling medium, while higher-energy electrons cross the gap, leaving behind a signal which depends on the initial angle and effects of multiple scattering in the sampling gap.

For the gas sampling calorimeter (Figure 20b), shower electron statistics are dominated by two larger components of nearly equal magnitude:

a) path length variations are much stronger in the gas sampling medium, because even the very soft shower electrons contribute, which are widely distributed in angle as they enter the sampling gap (Fischer 1978);

b) fluctuations in the rate of energy loss dE/dx (Landau fluctuations) become important in thin layers of gas.

The resolution of gas proportional calorimeters can be somewhat improved by limiting the path length variations. This is achieved by inserting thin metal walls between anode wires or by using proportional tubes of small cross-sectional area (Fischer 1978, Ludlam et al 1981). Recent investigations of gas mixtures (Atač et al 1981b) have demonstrated the feasibility of a "limited streamer" mode in which avalanches remain localized within a few tenths of a millimeter. A calorimeter of this type has given linear response over an extended energy range, with resolution $\sigma/E \simeq 17\%/\sqrt{E}$ for electrons (private communication, Atač 1981).

While the proportional wire calorimeter gives poorer resolution for electromagnetic showers, the enhanced fluctuations in its response are still small compared to the intrinsic fluctuations in hadron cascades. The choice of gas sampling calorimeters for hadron measurements can, in principle, be made without compromising energy resolution. This is not expected to be the case for uranium calorimeters, for which, however, no measurements with a gaseous sampling medium have been made so far.

With these types of detectors, spatial segmentation and localization can be easily implemented. This may be achieved in a projective geometry using strips or in a "tower" arrangement, e.g. by measuring the signal charge induced on a pattern of cathode pads. The tower arrangement is valuable for reducing ambiguities and confusion in multiparticle events. For this construction the proportional tubes are made from graphite-impregnated plastic with a sheet resistivity of $\sim 100\ k\Omega$/pad (Battistoni et al 1980, Ayres et al 1981).

Another technique currently being studied for achieving a very high degree of spatial segmentation is the so-called "drift-collection" calorimeter (Fischer & Ullaland 1980, Price & Ambats 1981). Shower electrons are collected on a relatively small number of proportional wire planes, with one shower coordinate determined by the drift time of ionization charge onto the collecting wires. A possible configuration is shown in Figure 21.

Gas sampling calorimetry in a digital mode (using Geiger, streamer, or flash-tube techniques) is a means for greatly simplifying the signal processing circuitry, and offers an expedient method for achieving a very high degree of segmentation.

Flash chambers consist of an array of tubular cells filled with a mixture of about 96% neon/4% helium; a pulsed high-voltage is applied across each cell after an external event trigger. In the presence of ionization charge, a signal-producing plasma discharge propagates over the full length of the cell. In one such array for a large neutrino experiment at Fermilab, 608 flash-chamber planes with a total of some 400,000 cells are sandwiched between absorber layers of sand and steel shot (Bogert et al 1981). The pattern of struck cells in each plane is read out by sensing induced signals on a pair of magnetostrictive delay lines. Figure 22 shows an on-line display of a high-energy neutrino

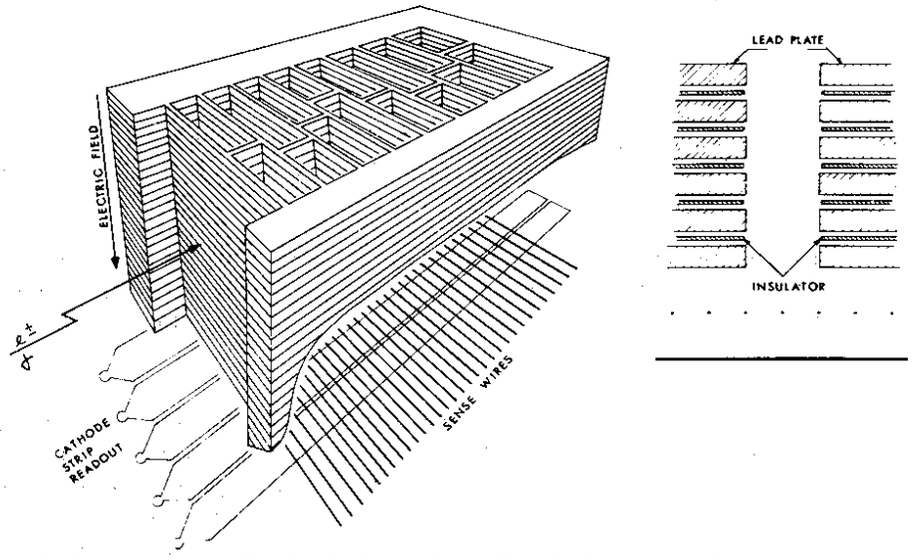

Figure 21 Geometrical arrangement for the high-density drift calorimeter. Cavities between absorber plates allow drifting of ionization electrons over long distances onto MWPC-type detector. Very high spatial granularity can be achieved at the cost of mechanical complexity and rate capability. A very uniform magnetic guidance field parallel to the drift direction is usually required (Fischer & Ullaland 1980).

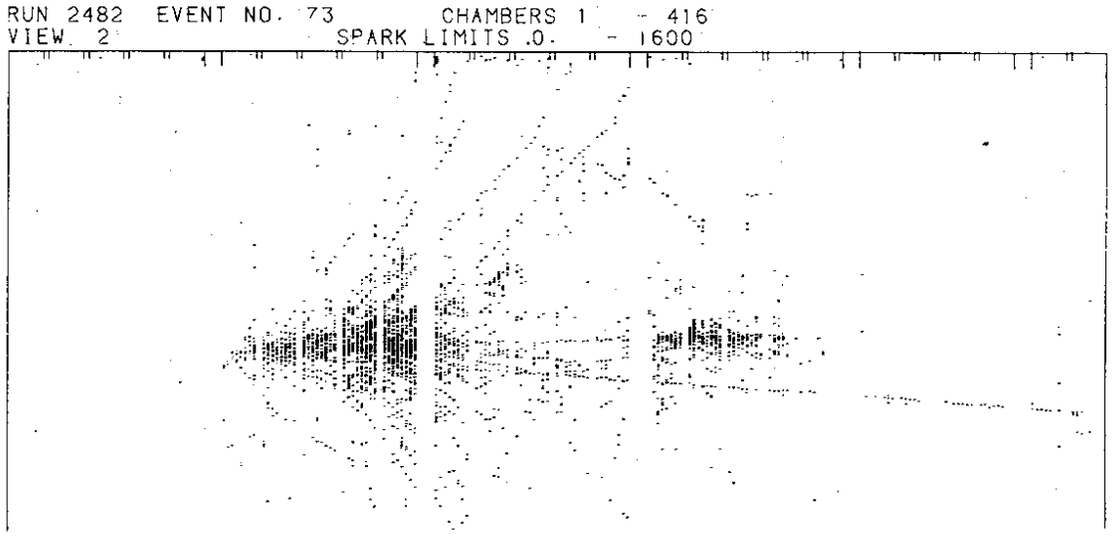

Figure 22 Display of high-energy neutrino event recorded by the flash chamber calorimeter of experiment 594 at FNAL (Bogert et al 1981).

event in the detector, with each dot representing a struck cell. The high degree of segmentation is evident. The energy response however is found to be non linear, indicating severe saturation effects for this type of digital readout at high energies.

Frequently, care is taken to limit the geometrical extension of the discharge region, usually accomplished with various mechanical discontinuities (beads, nylon wires, etc.). A calorimeter operated in this mode gave an energy resolution of $\sigma \simeq 12\%/\sqrt{E}$ for electron energies up to 5 GeV (private communication, Carithers 1981). This is much better than is normally achieved for gas sampling calorimeters, reflecting the absence of Landau and path-length fluctuations. At higher energies the calorimeter showed saturation effects due to the increasing probability for multiple hits over the geometrical extension of the discharge region.

6. OUTLOOK

The use of calorimetric methods in high-energy physics began with rather specialized applications, which capitalized on some unique features not attainable with other techniques: electromagnetic shower detectors for electron and photon measurements, neutrino detectors, and muon identifiers.

The evolution towards a more general detection technique — similar in scope to magnetic momentum analysis — had to wait for the development of hadronic calorimetry. Although the application of this technique to the hadron machines (which were inaugurated in the early 1970's) was delayed, it has shaped the detectors for the new CERN $p\bar{p}$ Collider and will be central to the detector facilities currently under discussion. At the same time, physics studies have evolved in a direction where measurements based on "classic" magnetic momentum analysis are supplemented or replaced by analyses which are based on very precise, global measurements of event structure, frequently requiring extraordinary trigger selectivity and which are much more suitable to calorimetric detection. For the next decade, physics studies will rely increasingly on these more global studies, with properties averaged over groups of particles and with the distinction between individual particles blurred unless they carry some very specific information. This role of calorimetry is sketched in Table 8.

Table 8 Future role of absorptive spectroscopy

Source of particles	Physics emphasis	Calorimeter properties	Technical implications
$pp(p\bar{p})$ collider	Rare processes: high p_T, lepton, photon production manifestations of heavy quarks, $W^{\pm}, Z^0, \ldots$	4πcoverage with e.m. and hadronic detection; high trigger selectivity	Approach intrinsic resolution in multicell device. Control of inhomogeneities, stability.
e^+e^- collider	Complex, high-multiplicity final states (multijets, electrons in jet, neutrinos)	Precision measurements of total, visible energy and momentum	Very high granularity; particle identification
Secondary beams $p \gtrsim 1$ TeV/c	Similar to first entry; with increasing energy, stronger emphasis on global features	Calorimeter becomes primary or sole spectrometer element	High granularity, high rate operation
Penetrating cosmic radiation; proton decay	Detailed final-state analysis of events with extremely low rate	Potentially largest detector systems ($\gtrsim$ 10,000 tons) with very fine grain readout	Ultra-low cost instrumentation

Despite recent conceptual and technical progress, a number of questions deserve further attention:

- What is the precise energy dependence of hadronic energy resolution?
- What improvement in energy, position, and angular resolution could be obtained with complete information on the individual shower distributions? With such information, can we tolerate increased longitudinal leakage without affecting energy resolution?
- What contributes to the measured energy resolution $\sigma(E) = 0.2\sqrt{E}$ of a fission-compensated hadron calorimeter?
- Can we understand hadronic sampling fluctuations to the same degree as we understand electromagnetic ones?
- Can particle identification and separation be improved if more detailed shower information is available?
- Are there advantages in mixing different absorber materials, or in changing the sampling step inside a calorimeter?

The very diverse applications of calorimetric techniques will ensure continued study of these and the many technical questions connected with the readout and signal processing of calorimeter information. There can *never* be a unique solution, but there should *always* be a search for the most suitable method. We hope that the information provided in this review will be useful towards this end.

Acknowledgements
We are indebted to many groups for providing us with information about their detectors and, in particular, to our collaborators in the R806/AFS groups at CERN, with whom a number of issues raised here were first discussed and tried. It is a pleasure to acknowledge the stimulation and interest arising from our association with W.J. Willis.

The progress we have reviewed here as well as the promise for the future is due in large measure to the support of calorimeter research by the program directors of many laboratories; we especially acknowledge the conviction and foresight with which such support has been rendered by the Experimental Facilities and Experimental Physics Divisions at CERN.

One of the authors (T.L.) is supported by the US Dept. of Energy under contract number DE-AC02-76CH00016.

Literature Cited

Abramowicz, H. et al 1981. *Nucl. Instrum. Methods* 180:429
Akopdjanov, G. A. et al 1977. *Nucl. Instrum. Methods* 146:441
Albrow, M. 1981. *General Meeting on LEP,* Villars, ed. M. Bourquin, p. 142. ECFA 81/54
Almehed, S. et al 1977. *CERN/ISRC/76–36*
Alvarez, L. W. 1968. *LRL Physics Note 672*
Amako, Y. 1981. *Proc. 1981 ISABELLE Summer Workshop,* BNL report 51443:1257
Amaldi, U. 1981. *Phys. Scripta* 23:409
Amendolia, S. R. et al 1980. *Pisa 80-4*
Anassontzis, E. et al 1981. *CERN/ISRC/81-16*
Anderson, R. L. et al 1978. *IEEE Trans. Nucl. Sci.* NS-25:340
Apel, J. et al 1975. *Nucl. Instrum. Methods* 127:495
Asano, Y. et al 1980. *Nucl. Instrum. Methods* 174:357
Astbury, A. 1981. *Phys. Scripta* 23:397
Atač, M. 1975. Ed. of *Proc. Calorimeter Workshop,*FNAL. Batavia, Ill.:FNAL
Atač, M. et al 1981a. *IEEE Trans. Nucl. Sci.* NS-28:500
Atač, M. et al 1981b. *Fermilab preprint FN-339,* to be published in *Nucl. Instrum. Methods*
Ayres, D. et al 1981. *Design report for Fermilab Collider Detector Facility*
Barloutaud, R. 1981. *Proc. Int. Conf. on High Energy Physics,* Lisbon, to be published
Baroncelli, A. 1974. *Nucl. Instrum. Methods* 118:445
Bartalucci, S. et al 1980. *Nucl. Instrum. Methods* 178:401
Bartel, W. et al 1979. *Phys. Lett.* 88B:171
Basile, M. et al 1979. *Nucl. Instrum. Methods* 163:93
Bathow, G. et al 1970. *Nucl. Phys.* B20:592
Battistoni, G. et al 1980. *Nucl. Instrum. Methods* 176:297
Baum, L. et al 1975. *Proc. Calorimeter Workshop,* FNAL, ed. M. Atač, p. 295. Batavia, Ill.:FNAL
Bég, M. A. B. 1981. *Rockefeller Univ. preprint 81-B-9,* and *Proc. EPS Int. Conf. on High Energy Physics,* Lisbon, to be published
Behrend, H. J. et al 1981. *Phys. Scripta* 23:610
Beron, B. L. et al 1973. *Proc. 5th Int. Conf. on Instrumentation for High-Energy Physics,* Frascati, p. 362. Frascati:CNEN
Binon, F. et al 1981. *Nucl. Instrum. Methods* 188:507
Blenar, G. et al 1981. *Proc. EPS Int. Conf. on High-Energy Physics,* Lisbon, to be published
Block, M. 1977. *Unpublished note UA1-26,* UA1 Collaboration (CERN)
Böck, R. et al 1981. *Nucl. Instrum. Methods* 186:533
Bogert, D. et al 1981. *IEEE Trans. Nucl. Sci.,* to be published
Bosio, C. et al 1978. *Nucl. Instrum. Methods* 157:35
Botner, O. 1981. *Phys. Scripta* 23:555
Botner, O., Fabjan, C.W. 1981.*Unpublished note,* AFS Collaboration (CERN)
Botner, O. et al 1981a. *IEEE Trans. Nucl. Sci.* NS-28:510
Botner, O. et al 1981b. *Nucl. Instrum. Methods* 179:45
Bouclier, R. et al 1980. *CERN-EP Internal Report 80–07*
Breidenbach, M. 1981. *Phys. Scripta* 23:507
Brisson, V. et al 1981. *Phys. Scripta* 23:688
Bromberg, C. 1979. *Phys. Rev. Lett.* 42:1202
Carithers, W. 1982. *BNL report 30321*
Chan, Y. et al 1978. *IEEE Trans. Nucl. Sci.* NS-25, 1:333
Charpak, G. et al 1978. *Physics Today,* Oct.:23
Chen, H. H. et al 1978. *Nucl. Instrum. Methods* 150:585
Cheshire, D. L. et al 1977. *Nucl. Instrum. Methods* 141:219
Clark, A. 1981. *Unpublished note,* UA2 Collaboration (CERN)
Clark, A. et al 1982. *The UA2 central calorimeter,* to be presented at the Int. Conf. on Instrumentation for Colliding Beam Physics, Stanford
Cobb, J. H. et al 1977. *Nucl. Instrum. Methods* 140:413
Cobb, J. H. et al 1979. *Nucl. Instrum. Methods* 158:93
Conversi, M. 1973. *Nature* 241:160
Conversi, M., Federici, L. 1978. *Nucl. Instrum. Methods* 151:193
Corden, M. J. et al 1982. *Phys. Scripta,* 25:5
Coyne, D. G. 1981. *SLAC-PUB 2809*

Cundy, D. et al 1976. *In Physics with very high energy e^+e^- colliding beams,* CERN 76-18:145
Davies-White, W. et al 1979. *Nucl. Instrum. Methods* 160:227
Della Negra, M. 1981. *Phys. Scripta* 23:468
Derenzo, S.E. et al 1974. *Nucl. Instrum. Methods* 122:319
Derrick, M. 1981. *Preprint ANL–HEP–CP–81–33,* Argonne, Ill.:ANL
Diakonou, M. et al 1979. *Phys. Lett.* 87B:292
Diddens, A.N. et al 1980. *Nucl. Instrum. Methods* 178:27
Doke, T. 1981. *Portugal Phys.* 12:9
Dris, M.A. 1979. *Nucl. Instrum. Methods* 161:311
Dris, M.A. et al 1979. *Phys. Rev.* D19:1361
Dydak, F. 1980. *Preprint CERN–EP/80–224*
Eckardt, V. et al 1978. *Nucl. Instrum. Methods* 155:353
Ellis, J. 1981. *Phenomenology of Gauge Theories,* CERN-TH 3174, and *Proc. Les Houches Summer School,* to be published
Erwin, A. et al 1975. *Proc. Calorimeter Workshop,* FNAL, ed. M. Atač, p. 271. Batavia, Ill.:FNAL
Fabjan, C.W. 1980. *ECFA–LEP Working Group,* ed. A. Zichichi, ECFA/79/39:191
Fabjan, C.W., Fischer, G.H. 1980. *Rep. Prog. Phys.* 43:1003
Fabjan, C.W., Willis, W.J. 1975. *Proc. Calorimeter Workshop,* FNAL, ed. M. Atač, p. 1. Batavia, Ill.:FNAL
Fabjan, C.W. et al 1975. *Phys. Lett.* 60B:105
Fabjan, C.W. et al 1977. *Nucl. Instrum. Methods* 141:61
Fabjan, C.W. et al 1981. *Nucl. Instrum. Methods* 185:119
Fischer, H.G. 1978. *Nucl. Instrum. Methods* 156:81
Fischer, H.G., Ullaland, O. 1980. *IEEE Trans. Nucl. Sci.* NS-27:38
Ford, R.L., Nelson, W.R. 1978. *SLAC–210*
Friend, B. et al 1976. *Nucl. Instrum. Methods* 136:505
Gabathuler, E. et al 1978. *Nucl. Instrum. Methods* 157:47
Gabriel, T.A. 1978. *Nucl. Instrum. Methods* 150:145
Gabriel, T.A., Amburgey, J.D. 1974. *Nucl. Instrum. Methods* 116:33
Gabriel, T.A. Schmidt, W. 1976. *Nucl. Instrum. Methods* 134:271
Garwin, R.C. 1960. *Rev. Sci. Instrum.* 31:1010
Georgi, H. et al 1974. *Phys. Rev. Lett.* 33:451
Goebel, K. et al 1973. *Nucl. Instrum. Methods* 113:433
Goldhaber, M., Sulak, L.R. 1981. *Comments Nucl. Part. Phys.* 10:215
Gordon, H.A. et al 1981. *Proc. 1981 ISABELLE Summer Workshop,* BNL 51443:884
Grannis, P.D. et al 1981. *Nucl. Instrum. Methods* 188:239
Grant, A. 1975. *Nucl. Instrum. Methods* 131:167
Hilke, H.J. 1981. *Proc. 1981 ISABELLE Summer Workshop,* BNL Report 51443:1275
Hitlin, D. et al 1976. *Nucl. Instrum. Methods* 137:225
Holder, M. et al 1978. *Nucl. Instrum. Methods* 151:69
Iwata, S. 1979. *Report DPNU–3–79.* Nagoya: the University
Jeffreys, P., Jensen, T. 1982. *Unpublished note,* AFS Collaboration (CERN)
Jones, W.W. 1969. *Phys. Rev.* 187:1868
Jonker, M. et al 1981. *Phys. Scripta* 23:677
Jonker, M. et al 1982. *Preprint CERN–EP/82–08*
Kadansky, V. et al 1981. *Phys. Scripta* 23:680
Kienzle, W. 1975. *CERN-NP Internal Report 75–12*
Kobayashi, M. et al 1981a. *Nucl. Instrum. Methods* 189:629
Kobayashi, M. et al 1981b. *Proc. Int. Symp. on Nuclear Radiation Detectors,* Tokyo, p. 465. Tokyo: INS, the University
Kourkoumelis, C. et al 1979. *Phys. Lett.* 81B:405
Kourkoumelis, C. et al 1980. *Z. Phys.* C5:95
Krishnaswamy, M.R. et al 1981. *Phys. Lett.* 106B:339
Kusumegi, A. et al 1981. *KEK 81–11,* to be published in *Nucl. Instrum. Methods*
Lederman, L. et al 1975. *Nucl. Instrum. Methods* 129:65
Longo, E., Sestili, I. 1975. *Nucl. Instrum. Methods* 128:283
Ludlam, T. et al 1981. *IEEE Trans. Nucl. Sci.* NS-28:517
Masuda, K. et al 1980. *Nucl. Instrum. Methods* 174:439
McDaniel, B.D. 1981. *Proc. 1981 Int. Symp. on Lepton and Photon Interactions at High Energies,* Bonn, ed. W. Pfeil., p. 921
Mueller, J.J. et al 1981. *IEEE Trans. Nucl. Sci.* NS-28:496

Murzin, V.S. 1967. *Progress in elementary particle and cosmic ray physics*, eds. J.G. Wilson and I.A. Wouthuysen, Vol. IX:247. Amsterdam:North-Holland
Panofsky, W.K.H. 1981. *Proc. 1981 Int. Symp. on Lepton and Photon Interactions at High Energies*, Bonn, ed. W. Pfeil, p. 957
Pati, H.C., Salam, A. 1974. *Phys. Rev.* D10:275
Picasso, E. 1981. *General Meeting on LEP*, Villars, ed. M. Bourquin, p. 32. ECFFA 81/54
Powel, B. et al 1981. *Preprint CERN-EP/81-144*, to be published in *Nucl. Instrum. Methods*.
Pretzl, K. 1981. *MPI-PAE/Exp.El. 95* and *Proc. of SLAC Summer Institute on Particle Physics*, Stanford
Price, L., Ambats, I. 1981. *IEEE Trans. Nucl. Sci.* NS-28:506
Radeka, V. 1977. *IEEE Trans. Nucl. Sci.* NS-24:293
Radeka, V., Williams, H. 1981. *Proc. 1981 ISABELLE Summer Workshop*, BNL 51443:1153
Ranft, J. 1972. *Particle Accel.* 3:129
Rishan, J.P. 1979. *SLAC 216*
Rosselet, L. 1981. *CERN 81-07:316*
Rossi, B. 1964. *High energy particles*, New York: Prentice Hall
Rossi, B., Staub, H. 1949. *Ionization chambers and counters*, New York: McGraw-Hill
Sauli, F. 1977. *CERN 77-09*
Schamberger, R.D. 1981. *Proc. 1981 Int. Symp. on Lepton and Photon Interactions at High Energies*, Bonn, ed. W. Pfeil, p. 217
Scharre, D. 1981. *Proc. 1981 Int. Symp. on Lepton and Photon Interactions at High Energies*, Bonn, ed. W. Pfeil, p. 163
Schönbacher, H., Witzeling, W. 1979. *Nucl. Instrum. Methods* 165:517
Selove, W. 1972. *CERN-NP Internal Report 72-25*
Selove, W. et al 1979. *Nucl. Instrum. Methods* 161:233
Selove, W. et al 1980. *Univ. Pennsylvania preprint UPR-75E*
Slattery, P. et al 1981. *Proc. Int. Conf. on High Energy Physics*, Lisbon, to be published.
Stevenson, J. et al 1981. *Nucl. Instrum. Methods* 188:41
Stone, S. 1981. *Phys. Scripta* 23:605
Stone, S. et al. 1978. *Nucl. Instrum. Methods* 151:387
Treille, D. 1981. *Preprint CERN-EP/81-134*
Van der Velde, J. 1981. *SLAC 239:457*
Vishnevskii, A.V. et al 1979. *Preprint ITEP-53*
Walker, R.L. et al 1981. *Preprint CALT-68-823*
Willis, W.J. 1972. *BNL 17522:207*
Willis, W.J. 1979. *Unpublished note*, AFS Collaboration (CERN)
Willis, W.J. 1981. *Preprint CERN-EP/81-21* and *Proc. Workshop on Future Relativistic Heavy Ion Experiments*, Darmstadt
Willis, W.J., Radeka, V. 1974. *Nucl. Instrum. Methods* 120:221
Willis, W.J., Winter, K. 1976. *In Physics with very high energy e^+e^- colliding beams*, CERN 76-18:131
Yoshimura, Y. et al 1976. *Nucl. Instrum. Methods* 137:57